Aerodynamic model development for general aviation aircraft based on flight test data

Đeverlija, Jan Juraj

Master's thesis / Diplomski rad

2021

Degree Grantor / Ustanova koja je dodijelila akademski / stručni stupanj: **University of Zagreb, Faculty of Mechanical Engineering and Naval Architecture / Sveučilište u Zagrebu, Fakultet strojarstva i brodogradnje**

Permanent link / Trajna poveznica: https://urn.nsk.hr/urn:nbn:hr:235:592022

Rights / Prava: In copyright/Zaštićeno autorskim pravom.

Download date / Datum preuzimanja: **2024-07-15**

Repository / Repozitorij:

Repository of Faculty of Mechanical Engineering and Naval Architecture University of Zagreb

UNIVERSITY OF ZAGREB

FACULTY OF MECHANICAL ENGINEERING AND NAVAL
ARCHITECTURE

MASTER'S THESIS

Jan Juraj Đeverlija

ZAGREB, 2021.

MASTER'S THESIS

AERODYNAMIC MODEL DEVELOPMENT FOR GENERAL AVIATION AIRCRAFT BASED ON FLIGHT TEST DATA

Mentor:

Prof. Dr. Sc. Milan Vrdoljak

Dr. Pierluigi Capone

Student:

Jan Juraj Đeverlija

To my family for being my biggest support and helping me through journey of academic part of life.

Statement | Izjava

I hereby declare that I have made this thesis independently using the knowledge acquired during my studies and the cited references.

Izjavljujem da sam ovaj rad radio samostalno koristeći znanja stečena tijekom studija i navedenu literaturu.

Zagreb, December 2021   Jan Juraj Đeverlija

Sveučilište u Zagrebu	
Fakultet strojarstva i brodogradnje	
Datum	Prilog
Klasa: **602 - 04 / 21 - 6 / 1**	
Ur.broj: **15 - 1703 - 21 -**	

DIPLOMSKI ZADATAK

Student: **Jan Juraj Đeverlija**   JMBAG: 0035199923

Naslov rada na hrvatskom jeziku: **Razvoj aerodinamičkog modela aviona opće avijacije temeljem podataka s testnih letova**

Naslov rada na engleskom jeziku: **Aerodynamic model development for general aviation aircraft based on flight test data**

Opis zadatka:

A flight test campaign was preformed by the Zürich University of Applied Sciences (ZHAW), Centre for Aviation in 2019 using the general aviation airplane Piper PA-28 equipped with necessary instruments. In these tests total of 150 maneuvers were recorded and these data can be used for the investigation and development of the aircraft model with the aim to improve existing aircraft simulator model as well as in other applications like handling quality assessment, control system analysis, investigation of aircraft modification, etc.

The flight test data recordings, after its processing and organizing, can be used for the estimation of aerodynamic coefficients for the chosen aerodynamic model. This model is also dependent on defined models of aircraft propulsion, inertia, weight and balance. A basic linear model was estimated previously but this model will be assessed and further improved. Flight trajectory can be also reconstructed from the measurements for the data compatibility check and for the estimation of sensor errors. Evaluation of the developed model can be done with its implementation in the ZHAW Research and Didactic Simulator and with simulation of selected flight test maneuvers.

Following tasks should be performed within the Thesis:

- Reevaluation of the flight test data to be used for parameter estimation;
- Improvement of the aircraft trajectory reconstruction;
- Review and improvement of the existing aerodynamic coefficients model.

Thesis should list used bibliography and any assistance received.

Zadatak zadan: Datum predaje rada: Predviđeni datumi obrane:

30. rujna 2021.   2. prosinca 2021.   13. – 17. prosinca 2021.

Zadatak zadao: Predsjednik Povjerenstva:

Prof. dr. sc. Milan Vrdoljak

Dr. Pierluigi Capone   Prof. dr. sc. Milan Vrdoljak

Acknowledgement

Contents

List of Figures

List of Tables

List of Symbols

Subscripts

Superscripts

Abbreviations

Sažetak

Ovaj diplomski radi nastavak je rada na projektu razvoja aerodinamičkog modela zrakoplova generalne avijacije, Piper PA-28, Centra za zrakoplovstvo Sveučilišta primijenjenih znanosti u Zürichu. Nakon prethodne obrade i organizacije podataka snimljenih tijekom leta, predstavljen je osnovni linearni model. U ovom diplomskom radu napravljeno je poboljšanje, ali prije samog rada na poboljšavanju modela, putem rekonstrukcije putanje leta potrebno je što preciznije obraditi model pogrešaka senzora. Velika pažnja posvećena je upravo tom dijelu. Završetkom rekonstrukcije putanje lete, s korigiranim vrijednostima senzora, primjenom linearne regresije metodom najmanjih kvadrata procjenjuju se aerodinamički parametri. Fokus je stavljen na uzdužno gibanje, poput sloma uzgona, dugo periodičnog i kratko periodičnog moda.

Ključne riječi: Piper PA-28, procjena parametara, aerodinamički koeficijenti, rekonstrukcija putanje leta, model pogrešaka senzora, linearna regresija, metoda pogreške izlazne varijable

Summary

This master thesis is a continuation of the work on a project of aerodynamic model development for a general aviation airplane, Piper PA-28, conducted by Centre for aviation at the Zürich University of Applied Sciences. After previous flight test data processing and organizing, a basic linear model was introduced. In this thesis its improvement was made, but before improvement itself, using flight path reconstruction it is necessary to develop sensor error model, as precisely as possible. Great attention is dedicated exactly to this part. Completion of the flight path reconstruction, with corrected sensor values, using linear regression aerodynamic parameters are estimated with ordinary least square method. Focus is put on longitudinal motion, such as stall, phugoid and short period manoeuvres.

Keywords: Piper PA-28, parameter estimation, aerodynamic coefficients, flight path reconstruction, sensor error model, linear regression, output-error method

Prošireni sažetak

Uvod

Jedan od projekata Centra za zrakoplovstvo (ZAV), Sveučilišta primijenjenih znanosti u Zürichu (ZHAW), je razvijanje aerodinamičkog modela aviona generalne avijacije Piper PA-28 (Slika 0.1) i njegova implementacija u simulator za istraživanje. Kako bi model u simulator bio što sličniji ponašanju letjelice u stvarnosti, cijeli model je temeljen na eksperimentalnim podacima snimljenih u letu. Za to je 2019. godine Centre for Aviation napravio kampanju testiranje leta u kojoj su snimljeni podaci iz različitih manevra. Simulator za primjenu ovog aerodinamičkog modela, ReDSim (Slika 0.2), razvili su zaposlenici zajedno sa studentima koji su svojim diplomskim radovima, odnosno završnim radovima, pridonosili razvoju i nalazi se u prostorijama sveučilišta u Winterthuru te stoji na raspolaganju studentima za projekte. Naravno simulator služi za provođenje laboratorijskih vježbi, a sam simulator nije ograničen na jednu letjelicu već omogućuje simulaciju letjelica različitih konfiguracije, od jedrilica do letjelica rotirajućih uzgonskih površina.

Na ovom projektu prethodno su već radili studenti i napisali svoje diplomske radove, [1], [2] i [3].

Slika 0.1: Piper PA-28-161 Warrior III [1]

   Glavni zadatak kojim se ovaj diplomski rad bavi je provjera i poboljšanje postojećeg modela aerodinamičkih koeficijenata. Kao što je strukturiran rad [3] na način da osoba koja će nastaviti s radom na projektu rad nastavlja u istom smjeru, tako je i ovaj diplomski rad strukturiran kao podloga za nastavak rada. Estimacija, odnosno procjena, parametara izvršava se linearnom regresijom, a odabrana metoda je metoda najmanjih kvadrata. Po završetku poboljšavanja modela slijedi njegova primjena u simulatoru na mjesto postojećeg modela PA-28, čime se model približava stvarnom ponašanju zrakoplova tijekom leta.

U ovom diplomskom radu prošireni su modeli aerodinamičkih koeficijenata koji su bili razvijeni u [3]. A prije rada na glavnom zadatku potrebno je bilo reevaluirati podatke koji se upotrebljavaju kod modeliranja te poboljšati rekonstrukciju trajektorije letjelice. U ovom proširenom sažetku nalazit će se, osim uvoda i zaključka, tri potpoglavlja. Čitatelja se svakako preporučuje na čitanje cijelog teksta radi boljeg razumijevanja.

Slika 0.2: Research and Didactic Simulator (ReDSim), Zurich University of
Applied Sciences [3]

Reevaulacija podataka

U jednom od prethodnih radova otkrivena je greška prilikom ugradnje inercijskog mjernog uređaja (IMU). Mjerni uređaj je bio postavljen na pod prostora za prtljagu koji se nalazi pod određenim kutom u odnosu na vodnu liniju. To uzrokuje greške kod komponenti linearnog ubrzanja, brzine promjene kutova i Eulerovih kutova.
Korekcija Eulerovih kutova vrši se pomoću matrice transformacije (0.1).

$$\mathbf{L}_{EB_{corr}} = \begin{bmatrix} \mathbf{L}_{EB_{corr}}(1,1) & ... & ... \\ \mathbf{L}_{EB_{corr}}(2,1) & ... & ... \\ \mathbf{L}_{EB_{corr}}(3,1) & \mathbf{L}_{EB_{corr}}(3,2) & \mathbf{L}_{EB_{corr}}(3,3) \end{bmatrix} \tag{0.1}$$

Vizualni prikaz korekcije Eulerovih kutova dan je slikom 0.3, na kojoj se nalazi jedan *dutch roll* manevar. Očekivano najveća promjena je kod kuta propinjanja θ. Korekcija greške vri se rotacijom oko y osi, zbog toga kut valjanja ϕ ostaje nepromijenjen, dok se kod kuta skretanja ψ nalaze male promjene.
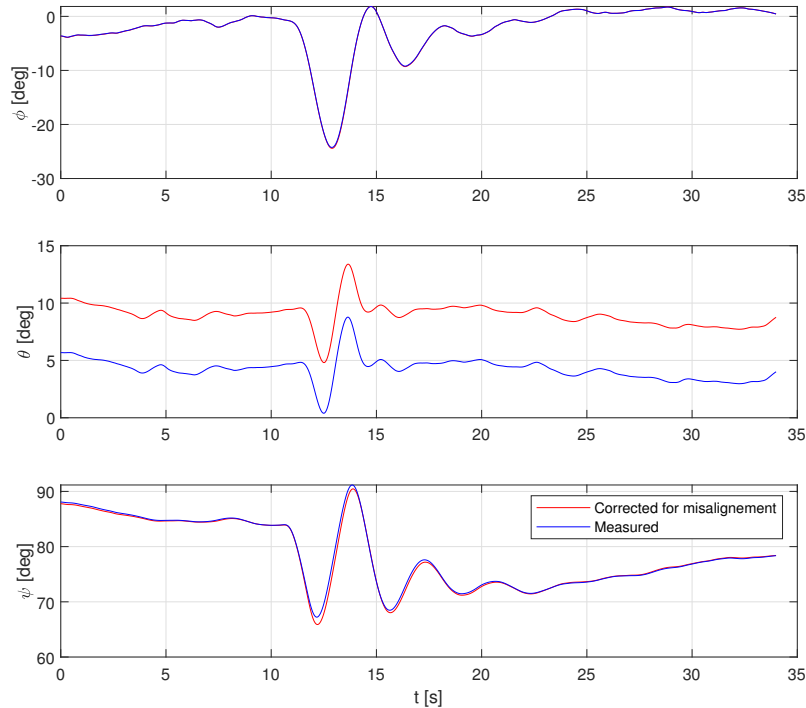
Slika 0.3: Primjer korekcije Eulerovih kutova

Rekonstrukcija trajektorije leta

Rekonstrukcija trajektorije leta potrebna je kako bi se osigurala konzistentnost i točnost mjerenih podataka pri aerodinamičkom modeliranju. U rekonstrukciji trajektorije potrebno je dobiti što točnije podudaranje krivulje rekonstruirane iz kinematskih jednadžbi s krivuljom mjerenih podataka. U ovom radu uspoređivani su: napadni kut α, kut klizanja β, brzina letjelice TAS eng. *True Airspeed*, brzina promjene kuta valjanja p, brzina promjene kuta propinjanja q, brzina promjene kuta skretanja r i visina leta h. Uz pomoć kinematskih jednadžbi dolazi se do vektora stanja (0.2), poglavlje 5.1..

$$\Delta x = [u, v, w, \phi, \theta, \psi, h] \tag{0.2}$$

Poznavanjem vektora stanja moguće je u svakom trenutku uspoređivati prethodno navedene veličine. Veličine koje nisu navedene u vektoru stanja izračunavaju se jednostavnim izrazima (0.3).

$$
\begin{aligned}
\alpha &= \tan^{-1}(w/u) \\
\beta &= \sin^{-1}(v/TAS) \\
TAS &= \sqrt{u^2 + v^2 + w^2}
\end{aligned}
\tag{0.3}
$$

Proces rekonstrukcije je iterativan i iziskuje veliku količinu vremena. Razvija se model pogreške senzora za tri veličine, α, β i TAS te se pojedinačno vrši se iteracija kroz sve manevre. Na 0.4 prikazana je shema koraka iteracije.
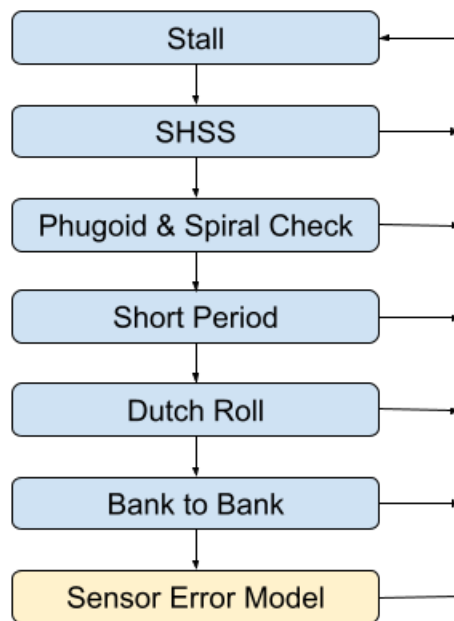
Slika 0.4: Shema koraka iteracije

Za rekonstrukciju se koristi skripta *fitlab*. Kao izlaz skripte je i "trošak" funkcije koji se treba minimizirati svakom iteracijom čime se postiže konvergencija rezultata. Ujedno se prikazuje i korelacija parametara, a u slučaju korelacije veće od |0.90| skripta ispisuje upozorenje i potrebno je izmijeniti model pogreške senzora.

Jedan od razvijenih modela je:

$$\beta_{recon} = b_\beta + k_\beta\beta \tag{0.4}$$

s parametrima prikazanim tablicom 0.1.

Tablica 0.1: Kut klizanja, parametri modela pogreške senzora

Parametar	Vrijednost	Mjerna jedinica	Značenje
b_β	$-8.0641 \cdot 10^{-3}$	rad	Istup kuta klizanja
k_β	0.984573	-	Nagib kuta klizanja

Slikom 0.5 prikazana je rekonstrukcija trajektorije letjelice za pet manevra sloma uzgona.
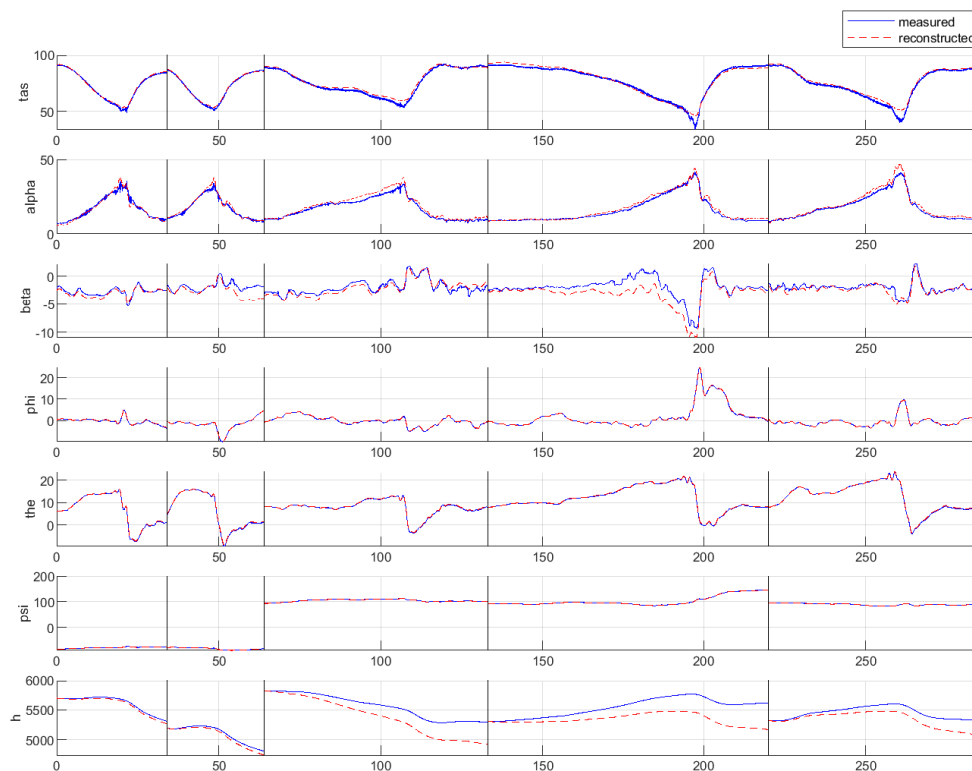
Slika 0.5: Rezultati rekonstrukcije trajektorije za pet manevra sloma uzgona

Na kraju je izvršena inverzija modela, opisana u 5.5..

Estimacija parametara aerodinamičkih koeficijenata

Posljednji zadatak bila je procjena parametara aerodinamičkih koeficijenata. Kao podloga koristili su se modeli razvijeni u [3] i oni su se proširili kako bi izračunati koeficijenti bili što bliži stvarnim vrijednostima. Jedan od razvijenih modela je model koeficijenta otpora C_D dan izrazom (0.5).

$$C_D = C_{D_0} + C_{D,\alpha^2}\alpha^2 + C_{L,\beta^2}\beta^2 + C_{D,C_T}C_T \qquad (0.5)$$

Vrijednosti koeficijenata iznose:

Tablica 0.2: C_D procijenjeni parametri

Parametar	Vrijednost	Mjerna jedinica	Relativna greška [%]
C_{D_0}	0.021746	–	0.17
C_{D,α^2}	1.3457	$1/\text{rad}^2$	0.07
C_{D,β^2}	0.21629	$1/\text{rad}^2$	0.16
C_{D,C_T}	0.33842	–	0.09

Podudaranje sa stvarnom vrijednosti koeficijenta otpora prikazano je slikom 6.14 na kojoj su prikazana pet manevra phugoida, četiri manevra sloma uzgona i šest manevra konstantnog pravca i konstantnog kuta klizanja.
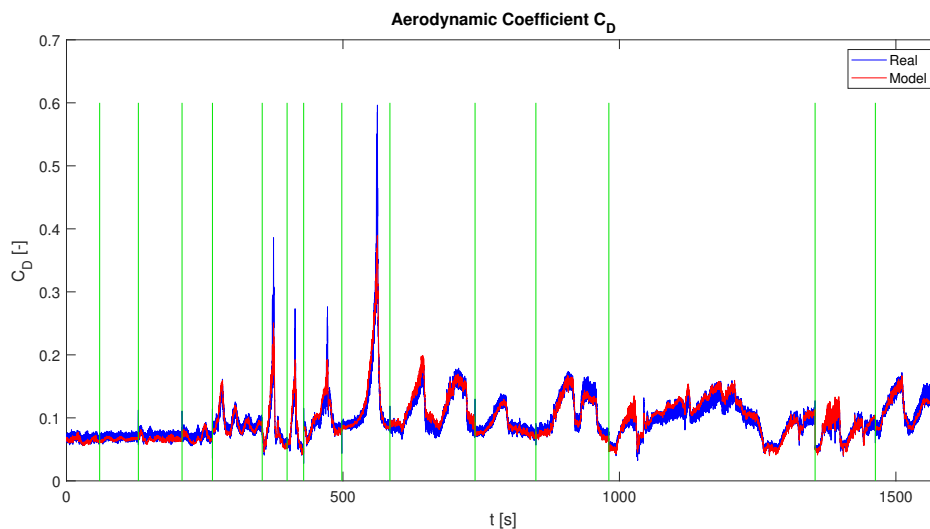
Slika 0.6: C_D model za odabrane manevre

Jedan od načina kako se mogu uočiti nedostaci razvijenog modela je analiza reziduala. Analizom je moguće prepoznati uzorke među prediktorima, u ovom slučaju to su α^2, β^2 i C_T, slika 0.7.
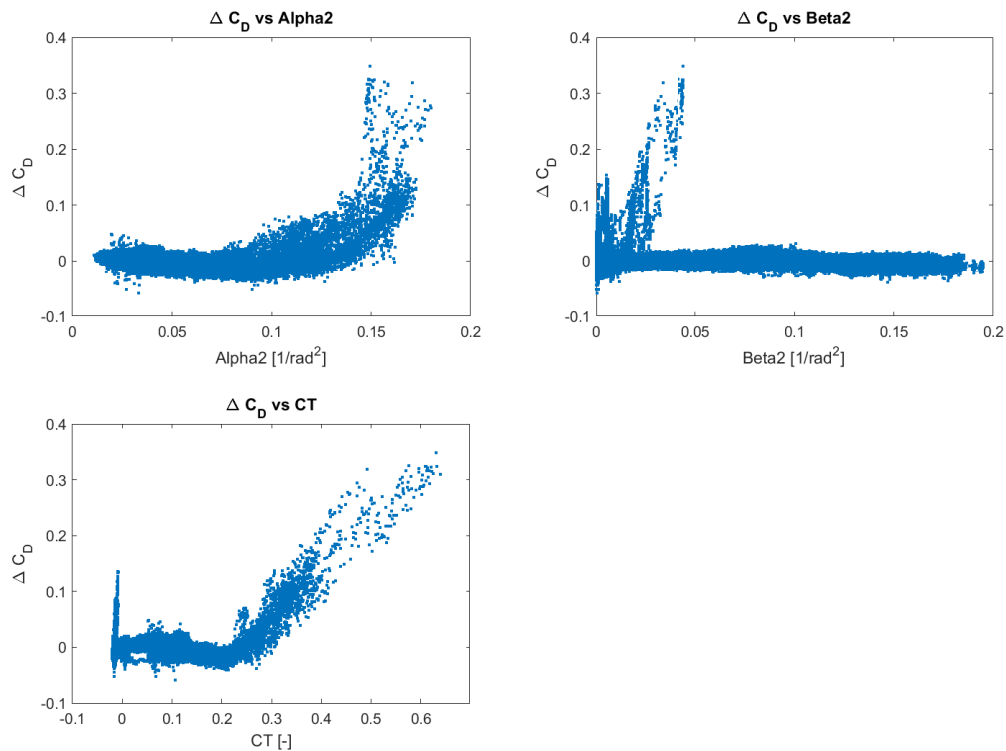
Slika 0.7: C_D reziduali u odnosu s prediktorima

Proširenje modela uglavnom dovodi do boljeg podudaranja krivulja, no kod procjene koeficijenta otpora to nije bio slučaj, što je vidljivo sa slike 0.8. U ovom slučaju vrijednosti procijenjenog koeficijenta otpora rastu i dodatno se povećava razlika između estimirane i stvarne vrijednosti. Prošireni model je detaljnije opisan u poglavlju 6.5.

Osim ovog modela razvijeni su još modeli koeficijenta momenta propinjanja i koeficijenta uzgona.
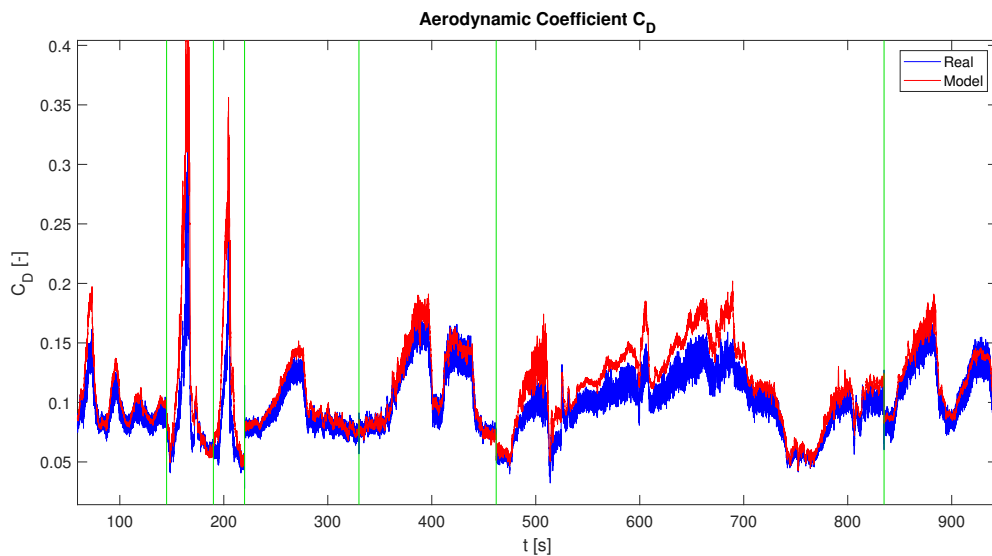
Slika 0.8: C_D prošireni model

Zaključak

Svrha ovog diplomskog rada je poboljšanje prethodno razvijenih modela aerodinamičkih koeficijenata. Kako je ovaj diplomski rad nastavak rada na projektu, osim provjere svih podataka i skripti koje se koriste, potrebno je bilo napraviti dodatne korake. Rad na projektu je izvršen tako da bude podloga za budući rad, tj. da osobe koje nastavljaju s radom na projektu to mogu jednostavno učiniti.

Nakon što su provjereni svi podaci, rekonstruirana je trajektorija leta. Time se provjerava točnost izmjerenih podataka potrebnih za aerodinamičko modeliranje. Postupak je završio s tri razvijena modela pogreške senzora.

U završnom dijelu poboljšani su modeli aerodinamičkih koeficijenata uzdužnog gibanja: koeficijent propinjanja C_m, koeficijent uzgona C_L i koeficijent otpora C_D.

Preostaje poboljšati prethodno razvijene modele aerodinamičkih koeficijenata bočnog gibanja. Osim toga, dodatno bi se mogli proširiti modeli uzdužnog gibanja, kao na primjer nelinearnom regresijom čime bi se obuhvatio slom uzgona. Razvijene modele aerodinamičkih koeficijenata uzdužnog i bočnog gibanja naposljetku potrebno je implementirati u ReDSim simulator.

1 | Introduction

One of projects of the Centre for Aviation (ZAV) at the Zürich University of Applied Sciences (ZHAW) is development of aerodynamic model of a general aviation aircraft, Piper PA-28 (Figure 1.1), and its implementation in the research simulator. In order for the model in the simulator to be as close as possible to the behaviour of actual aircraft, the whole model is based on experimental data recorded during flight. For that reason, in 2019. Centre for Aviation carried out a flight test campaign in which different manoeuvres were performed. The simulator in which this model is to be implemented, ReDSim (Figure 1.2), was developed by employees together with students who contributed in scope of their master or bachelor thesis and is located in the premises of the university in Winterthur and is available to students for projects. Of course, the simulator serves for laboratory exercises and the simulator itself is not limited to a specific aircraft, but is capable of simulating aircrafts of different configuration, form sailplanes to rotary wing aircrafts.

Figure 1.1: Piper PA-28-161 Warrior III [1]

Main task of this master thesis is review and improvement of existing aerodynamic coefficient models. Parameter estimation is done with linear regression using least squares method. In the end the model is to be implemented in the simulator, getting one step closer to recreating the actual behaviour of the aircraft.

Figure 1.2: Research and Didactic Simulator (ReDSim), Zurich University of Applied Sciences [3]

1.1.   Thesis Scope

After two master thesis [1] and [2] dealt with raw flight test data, another master thesis project [3] continued the work in aim of preparing the data and setting up the basis for parameter estimation of the aerodynamic coefficients.

This thesis begins with re-evaluation of the flight test data. All the scripts, used to generate data, are to be validated to make sure that the correct data is used. In order to carry out data compatibility check, improvement of the aircraft trajectory reconstruction will be done. Meaning that the quality of the recorded data is going to be improved. Already implemented basic aerodynamic model becomes more suitable to be built upon which will result in having a model in simulator with behaviour closer to the actual aircraft. It should be noted that engine model as well as mass and balance were left untouched, as it was agreed that the accuracy of these models was sufficient. Some aerodynamic models are extended with nonlinear terms. There was a great desire to estimate parameters with nonlinear regression, however due to shortage of time that was not pursued.

1.2.   Thesis Structure

As previous students working on this project have written their thesis, this one will also be structured in a way that the work done is easily readable and understandable. Making sure that it is again a solid foundation so that the students who will be working on this project in the future can straightforwardly continue the model improvement.

General aircraft data and specialized measuring equipment are found in chapter 2., along with what is being recorded in a flight test.

Chapter 3. contains theory of system identification including what needs to be done during the process, necessary steps and methodology followed. Besides that, in section 3.2. conventions for aerodynamic forces and moments, control surfaces deflections and coordinate system are defined.

Subject of chapter 4. is correction of flight test data where an issue with device alignment is dealt with.

Then comes chapter 5., also known as data compatibility check. Here it is made sure that the data is consistent and without errors. Aim of this chapter is to improve recorded

data. It contains a short method introduction followed by description of the trajectory reconstruction process itself. After sensor error models are developed, results are shown for all manoeuvres.

All that leads to chapter 6. in which aerodynamic coefficient models are developed using linear regression for which a quick introduction is included.

Lastly the thesis is completed with a conclusion in chapter 7.

All codes are written in *MATLAB*. Used script, functions and all data used can be found in appendix A.

2 | Test Aircraft and Instrumentation

2.1. Test Aircraft

To familiarize the reader with the test aircraft shown in Figure 2.1, few words about it for the beginning. Piper PA-28 Warrior III, registration HB-PRL of *Ausserschwyzer Fluggemeinschaft* located in Wangen, Switzerland, is a single-engine (*Lycoming O-320-D3G*) with two-blade fixed pitch propeller and fixed landing gear (tricycle configuration) monoplane. It is all-metal, unpressurized with low-mounted wings. Three-view of the test aircraft can be seen in Figure 2.2 with general dimensions presented in table 2.1.

Figure 2.1: Test aircraft, Piper PA-28 Warrior III, HB-PRL [1]
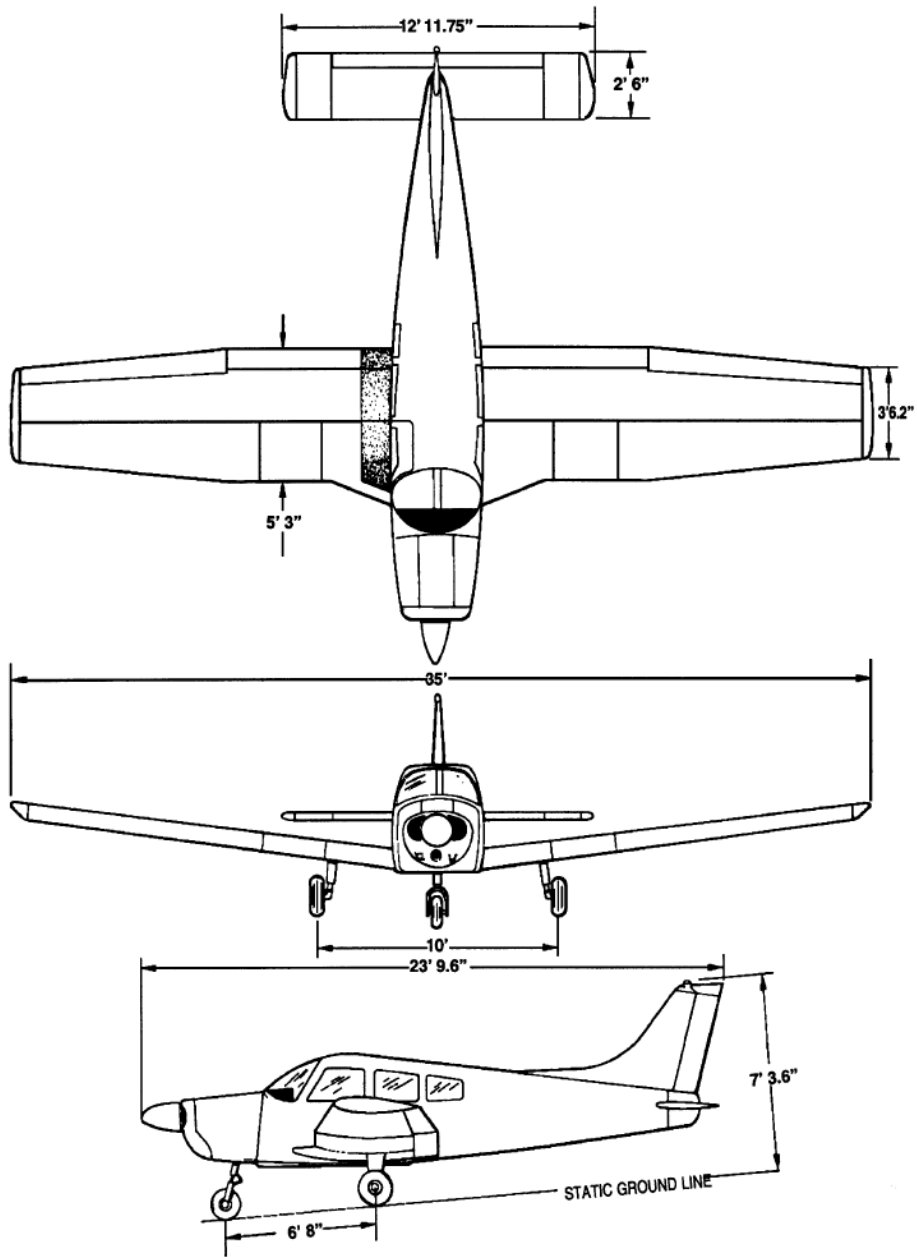
Figure 2.2: Three-view of Piper PA-28 Warrior III [4]

Table 2.1: Piper PA-28 Warrior III general dimensions

Dimension	Symbol	Value
Aircraft length	-	7.25 m
Aircraft height	-	2.23 m
Wingspan	b	10.67 m
Wing root chord length	c_r	1.60 m
Wing tip chord length	c_t	1.07 m
Mean aerodynamic chord	$\bar{c}$	1.602 m
Wing surface reference area	S_{ref}	15.8 m^2
Wing aspect ratio	AR	7.24
Propeller diameter	D	1.88 m

2.2.   Flight Test Data Overview

This section will provide a quick overview of how the data was acquired. It is an important step because of one specific rule: *"If it is not in the data, it cannot be modelled."*. Meaning that unknown system parameters could not be efficiently extracted due to the limits set by gathered data in terms of scope and accuracy. Avoiding this issue is done with three important aspects:

1. Defined scope of the flight test,

2. Defined suitable sequence of flight manoeuvres being performed at each test point,

3. Choosing adequate form of the inputs to excite the aircraft motion in some optimum sense [5].

A total of 159 test points were conducted in span of nine test flights. To record in-flight data, with the respect of said above, the aircraft needs to be equipped with specialized instrumentations and sensors.

2.2.1.   Specialized equipment

First on the list is the Air Data Boom (ADB), shown in Figure 2.3. It's an instrument which measures the Angle of Attack (AoA), Angle of Sideslip (AoS), static and total pressure. To obtain data as precisely as possible it is necessary to place the instrument the field of free stream, at the tip of an aircraft wing or at the nose of an aircraft. In this case the ADB was mounted at the right wing tip.

Figure 2.3: Air Data Boom (ADB) [1]

Next important instrument is the Inertial Measurement Unit (IMU) visible in Figure 2.4, which measures angular rates and linear accelerations. Besides that, there are two GPS antennas located on top of the fuselage that gather the GPS position.

Figure 2.4: Inertial Measurement Unit (IMU) [2]

Recording of all sensor signals, apart from the IMU, is done with Real-Time Embedded Industrial Controller (cRIO), seen in Figure 2.5, on which the data is saved and then extracted for post-processing. Both the IMU and cRIO units are positioned in the aircraft's luggage compartment.

Figure 2.5: Real-time embedded industrial controller (cRIO)

Other equipment installed:

- RPM sensor measuring the engine speed,

- Temperature sensors gathering Outside Air Temperature (OAT), that is the ambient air temperature at current altitude,

- Hygrometer measuring air humidity,

- String potentiometers measuring deflections of aircraft control surfaces, i.e. aileron, rudder and elevator and also their trim tab positions,

- Stick force sensor gathering forces that pilot exerts on the aircraft control wheel,

- Sound recorder, video cameras, marker switch, pressure transmitters, power supply.

After installation of the equipment and before the actual flight testing it is required to have a detailed plan of flight test itself. Specific manoeuvres allow for specific data to come in focus, used in further analysis. That is why during flight test a different set of manoeuvres are performed. In this test campaign manoeuvres performed were: stall, phugoid, spiral check, short period pitch oscillation, steady heading steady sideslip, dutch roll, level turn, bank to bank roll, take-off, climb and landing.

This was just a brief look of the aircraft itself and equipment used for recording the flight test data. In-depth look of the instrumentation and the procedure of data collection is found in [1] and [2].

3 | Theoretical Background

3.1. System Identification

General problem of this master thesis falls in a broader category of scientific discipline called system identification. What system identification is concerned with is obtaining the knowledge of a physical system. Observing the system and then providing a description of it is an inverse problem. It is understood that system identification is occupied with deriving a mathematical model from experimental data, for that reason its application spans every possible field. First thing that comes to mind is engineering like mechanical or civil, but it advances from medicine and biology to economics and others. Subject of this thesis belongs to a group called flight vehicle identification.

In most cases, no matter how detailed mathematical model describing behaviour of, in this case an aircraft, is, it exhibits a simplified system as the real process is too complex. Instead of expanding the model in effort to define real process it is always better to follow an expression, *"as simple as possible, and as complex as necessary"*.
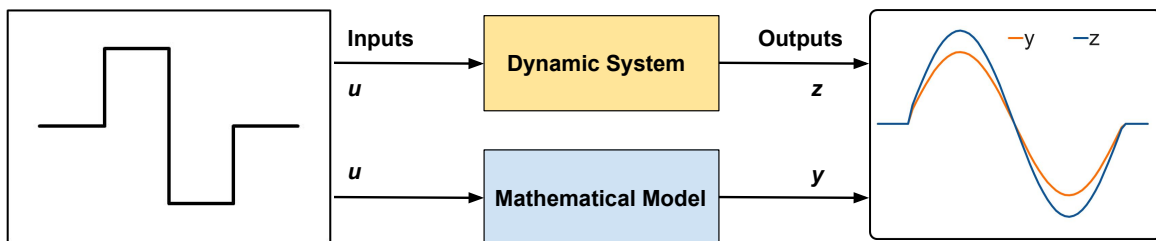
Figure 3.1: Dynamic system schematic, based on [5] and [6]

Figure 3.1 is presenting a visual representation of system identification. Defining the system in state space is done with an input u, passed into both dynamic system block, representing the real dynamics of an aircraft, and mathematical model block, representing the simulation model of said dynamic system, yielding in outputs z and y. Ideally the measured aircraft response z, the measured data, and simulated response y are equal but, as stated before, given the complexity there will always be difference. Determining a mathematical model sufficiently is done using unknown parameters, indirectly coming from measured data. For that, a system is provided with inputs and then appropriate responses are obtained. Obtained is a better fitting word than recorded, as the aerodynamic forces and moments, for example, acting on the aircraft are not measured directly yet they are derived from other measured data.

Quantifying numeric values of unknown parameters is a segment of model building process known as *parameter estimation*. This process is followed by model validation, which is necessary to validate the accuracy of derived mathematical model. Not being accurate enough, calls for a change in model structure and the process is repeated. It is obvious that system identification is an iterative process where available data might not be sufficient, demanding new experimental data as well as expanding the model structure. Entangled process of system identification, parameter estimation and simulation is presented in Figure 3.2.

Model structure
and parameters
known a priori

Simulation

Concerned with the
computation of system
responses

Numerical integration

Model structure
and parameters
unknown

Model structure
fixed

Parameter estimation

Concerned with the
quantification of
parameter values

Statistical estimation of
parameters

System identification

Concerned with the model
structure determination
and estimation of
parameters

Figure 3.2: System identification, parameter estimation and simulation definition, figure is based on [5]

Background of mathematical model is of highest importance. In flight vehicle system identification predominately the model is phenomenological, meaning that the model stems from basic principles and theoretical formulation of physics of the process. Parameters have physical interpretation described with ordinary or partial differential equations. The whole process can be divided into subprocesses and each of it having detail description helps in overall understanding of observed process. Apart from that, system identification provides the ability for producing flight simulators with numerous applications, like pilot training.

Aircraft parameter estimation relies on flight-test techniques, instrumentation and methods of data analysis. A methodology called *Quad-M*, Figure 3.3, is derived from covering these topics. It is comprised of: manoeuvre, measurement, method and model.
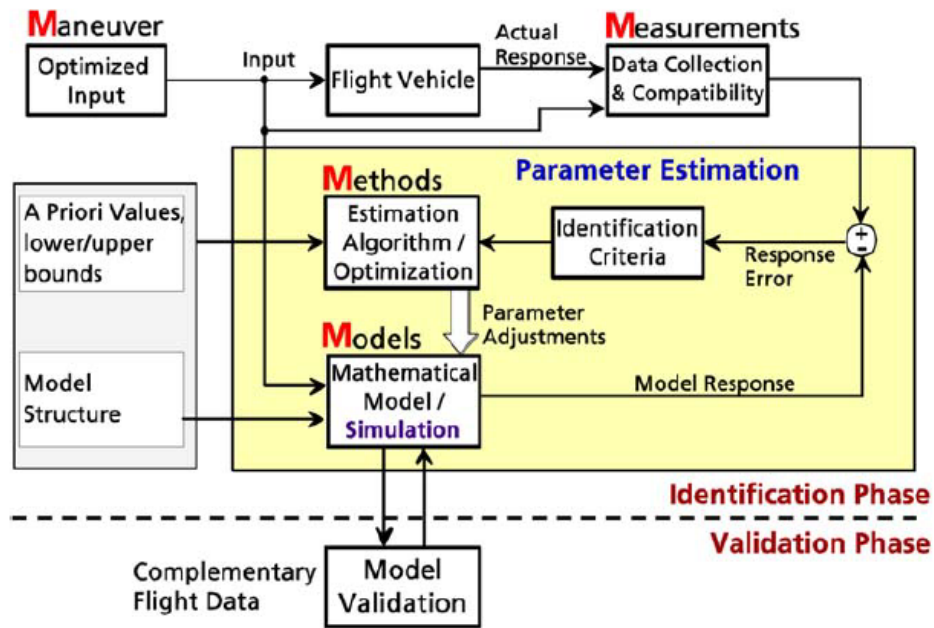
Figure 3.3: Quad-M methodology [5]

For successful flight vehicle system identification, each of the interdependent topics needs to be carefully considered. Following the listing order, first "M" described is *Manoeuvre*. Developing desired model information through whole flight envelope needs to be gathered. For that reason, manoeuvres are to be selected to fulfil that. Achieving that is possible with quality *Measurement*, i.e. use of the right equipment and filters to collect and processing data. Third "M" is *Method* implying that analysing data depends on method choice. Some methods for application need to be adapted in regards to data available. Lastly *Model* structure is directly correlated to the type of flight vehicle.

3.2. Conventions

As stated before, this thesis is continuation of work on a project, therefore the conventions defined are not changed. Figure 3.4 showing an aircraft in flight, presents used conventions.
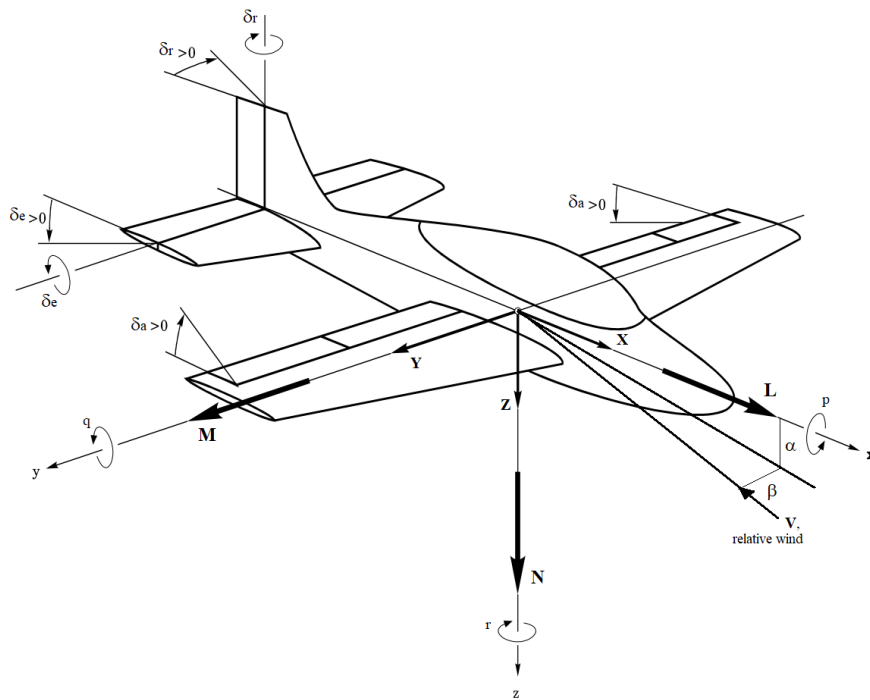
Figure 3.4: Body coordinate system (BCS), figure from [7]

Control surfaces deflection:

- δ_a Aileron deflection - positive deflection on right wing is aileron up and on the left wing is aileron down. Instead of having two deflections, arithmetic mean of both aileron deflections was introduced with positive deflection being aileron up.

- δ_e Elevator deflection - positive deflection is elevator down,

- δ_r Rudder deflection - positive deflection is rudder to the port side.

Moments M, N are positive when control surface's deflection is negative. Roll moment L is positive when starboard (right) wing goes down. For arithmetic mean of aileron, roll moment is positive for negative deflection.

4 | Flight Test Data Correction

Re-evaluation of the data started with reprocessing raw data as it was necessary to check weather already implemented sensor error models were influencing the data. More about sensor error model and what it does is discussed later in this chapter.

Also flight test data required a correction due to IMU installation error discovered in [2] during flight path reconstruction. The IMU was installed in the luggage compartment, but due to the slope of the floor there was an angle in respect to the aircraft's water line as seen in Figure 4.1. That calls for correction of linear accelerations, angular rates and Euler angles.

Since linear accelerations and angular rates correction was done previously, here Euler angles correction is emphasized.
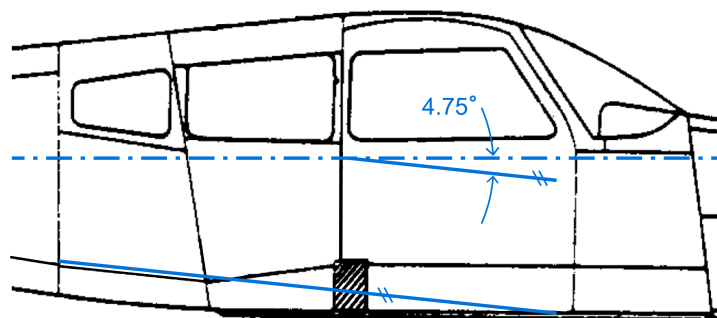
Figure 4.1: Luggage floor slope in respect to aircraft's water line [3]

4.1.   Attitude Angle Correction

Euler angles represent a sequence of transforming from one coordinate system, fixed Earth axis, to a moving coordinate system, body axis. The transformation is done with three rotation matrices, each around a different coordinate axis:

$$\mathbf{L}_{BE} = \mathbf{L}_x(\phi_m)\mathbf{L}_y(\theta_m)\mathbf{L}_z(\psi_m) \tag{4.1}$$

where

$$\mathbf{L}_x(\phi_m) = \begin{bmatrix} 1 & 0 & 0 \\ 0 & \cos\phi_m & \sin\phi_m \\ 0 & -\sin\phi_m & \cos\phi_m \end{bmatrix} \tag{4.2}$$

$$\mathbf{L}_y(\theta_m) = \begin{bmatrix} \cos\theta_m & 0 & -\sin\theta_m \\ 0 & 1 & 0 \\ \sin\theta_m & 0 & \cos\theta_m \end{bmatrix} \tag{4.3}$$

$$\mathbf{L}_z(\psi_m) = \begin{bmatrix} \cos\psi_m & \sin\psi_m & 0 \\ -\sin\psi_m & \cos\psi_m & 0 \\ 0 & 0 & 1 \end{bmatrix} \tag{4.4}$$

Misalignment of the IMU can be represented by adding additional rotation $\mathbf{L}(\Delta\theta)$, where $\Delta\theta$ represents the angle of the misalignment. In [3] it was measured that the misalignment is $\Delta\theta = 4.75°$.

$$\mathbf{L}(\Delta\theta) = \begin{bmatrix} \cos\Delta\theta & 0 & -\sin\Delta\theta \\ 0 & 1 & 0 \\ \sin\Delta\theta & 0 & \cos\Delta\theta \end{bmatrix} \tag{4.5}$$

Transformation matrix then becomes:

$$\mathbf{L}_{BE_{corr}} = \mathbf{L}(\Delta\theta)\mathbf{L}_x(\phi_m)\mathbf{L}_y(\theta_m)\mathbf{L}_z(\psi_m) \tag{4.6}$$

Inversion of (4.6) leads to transformation from body to Earth axes:

$$\mathbf{L}_{EB_{corr}} = \mathbf{L}_{BE_{corr}}^{-1}. \tag{4.7}$$

Final transformation matrix is expressed in (4.8). Due to shortage of space, terms of matrix used in correction of the measured Euler angles will be written out outside of the array:

$$\mathbf{L}_{EB_{corr}} = \begin{bmatrix} \mathbf{L}_{EB_{corr}}(1,1) & ... & ... \\ \mathbf{L}_{EB_{corr}}(2,1) & ... & ... \\ \mathbf{L}_{EB_{corr}}(3,1) & \mathbf{L}_{EB_{corr}}(3,2) & \mathbf{L}_{EB_{corr}}(3,3) \end{bmatrix} \qquad (4.8)$$

$$\mathbf{L}_{EB_{corr}}(1,1) = \cos\theta_m \cos\psi_m \cos\Delta\theta - \cos\phi_m \sin\theta_m \cos\psi_m \sin\Delta\theta ...$$
$$- \sin\phi_m \sin\psi_m \sin\Delta\theta$$

$$\mathbf{L}_{EB_{corr}}(2,1) = \cos\theta_m \sin\psi_m \cos\Delta\theta - \cos\phi_m \sin\theta_m \sin\psi_m \sin\Delta\theta ...$$
$$+ \sin\phi_m \cos\psi_m \sin\Delta\theta \qquad (4.9)$$

$$\mathbf{L}_{EB_{corr}}(3,1) = -\sin\theta_m \cos\Delta\theta - \cos\phi_m \cos\theta_m \sin\Delta\theta$$

$$\mathbf{L}_{EB_{corr}}(3,2) = \sin\phi_m \cos\theta_m$$

$$\mathbf{L}_{EB_{corr}}(3,3) = -\sin\theta_m \sin\Delta\theta + \cos\phi_m \cos\theta_m \cos\Delta\theta$$

Corrected Euler angles are obtained from relationships:

$$\phi_{corr} = \tan^{-1}(\mathbf{L}_{EB_{corr}}(3,2), \mathbf{L}_{EB_{corr}}(3,3))$$
$$\theta_{corr} = \sin^{-1}(-\mathbf{L}_{EB_{corr}}(3,1)) \qquad (4.10)$$
$$\psi_{corr} = \tan^{-1}(\mathbf{L}_{EB_{corr}}(2,1), \mathbf{L}_{EB_{corr}}(1,1))$$

Only when the correction is done it can be said that the values in body coordinate system are accurate. In appendix A.2. the reader will find the MATLAB script used to correct the data for this problem.

4.1.1.   Misalignment effect

Getting a grip on what effect does the IMU misalignment have, is best in a visual overview. Figure 4.2 shows how Euler angles before and after correction, while Figure 4.3 shows linear accelerations and rotational rates correction. Note that both figures represent only one manoeuvre, a dutch roll, and the accelerations and rates are filtered with a low-pass filter. More about filtering flight test data parameters can be found in [3].
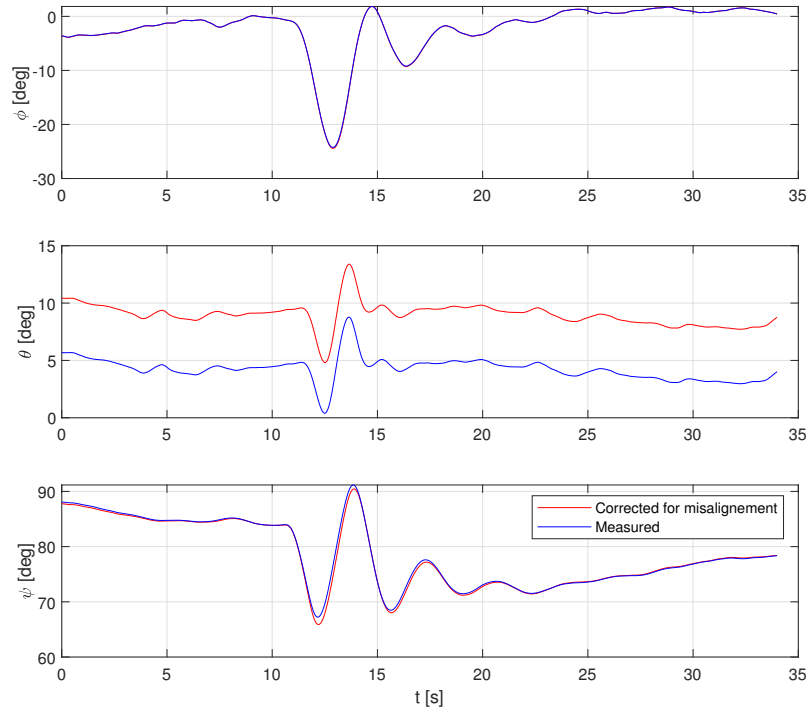
Figure 4.2: Euler angles correction for misalignment
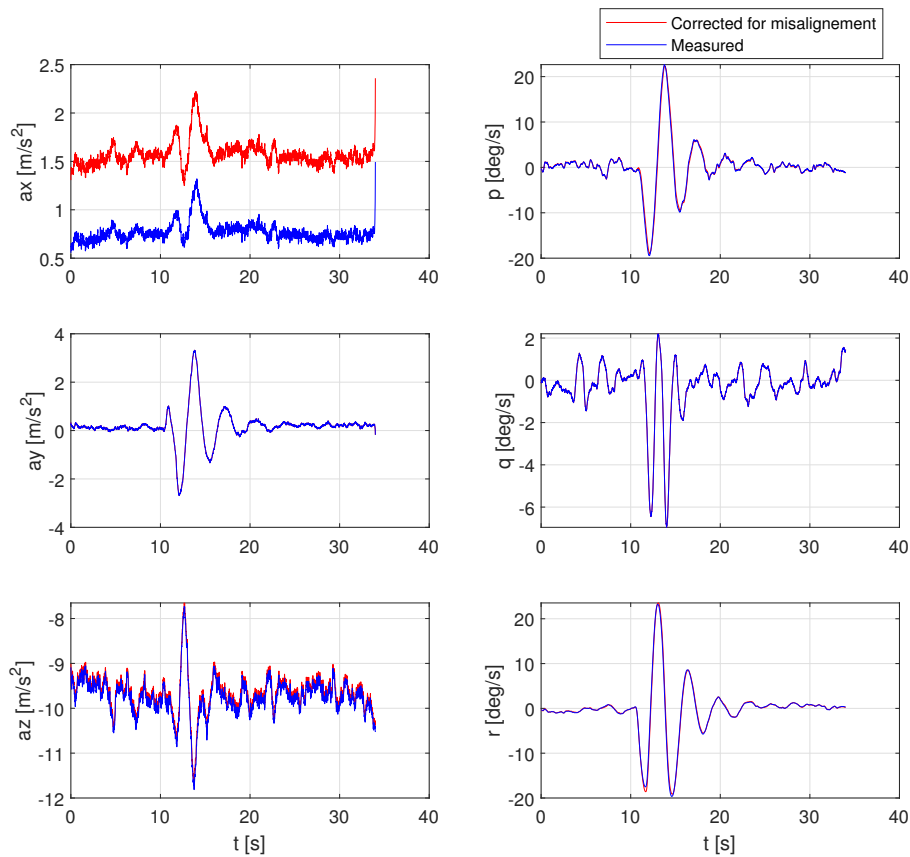
Figure 4.3: Linear accelerations and rotational rates correction for misalign-
ment

For Euler angles, as expected, the biggest difference has pitch angle θ, a difference in yaw angle ψ is also present while the roll angle ϕ does not change. When observing the linear accelerations it's easy to notice is that acceleration in y axis is exactly the same as measured, that is clear since the rotation of the Euler angles is performed about that axis. For the same reason, pitch rate is the same before and after correction.

5 | Flight Path Reconstruction

Measured data used for aerodynamic modelling needs to be consistent and without corruption, i.e. errors. That is why step called Flight Path Reconstruction (FPR) is required with the aim of improving recorded data. Reconstructing aircraft's trajectory is a process of matching measured states with reconstructed, obtained with kinematic equations. States being compared in this thesis are:

- Angle of Attack, α

- Angle of Sideslip, β

- True Airspeed, TAS

- Roll rate, p

- Pitch rate, q

- Yaw rate, r

- Altitude, h

5.1. Kinematic Equations

Before explaining data comparison for FPR, a quick overview of kinematic equations being used will be shown as these equations will be needed for data comparison.

Translational equations of motion in BCS (5.2) with the assumption of thrust components (5.1) are derived from observing airplane flight in a state of equilibrium with the hypothesis of a rigid body.

$$\mathbf{T} = \begin{bmatrix} T\cos\alpha_T \\ 0 \\ T\sin\alpha_T \end{bmatrix} \tag{5.1}$$

$$\dot{u} = rv - qw + \frac{T\cos\alpha_T}{m} + \frac{X}{m} - g\sin\theta$$
$$\dot{v} = -ru + pw + \frac{Y}{m} + g\cos\theta\sin\phi \tag{5.2}$$
$$\dot{w} = qu - pv + \frac{T\sin\alpha_T}{m} + \frac{Z}{m} - g\cos\theta\cos\phi$$

Linear accelerations can be explicitly noted:

$$a_x = \frac{T\cos\alpha_T}{m} + \frac{X}{m}$$
$$a_y = \frac{Y}{m} \tag{5.3}$$
$$a_z = \frac{T\sin\alpha_T}{m} + \frac{Z}{m}$$

where $[X, Y, Z]^T$ is aerodynamic force vector in body coordinate system.

Angular rates equations are shown in (5.4). Last thing missing is the position equation, (5.5). Equations are obtained from [8].

$$\dot{\phi} = p + (\sin\phi\tan\theta)q + (\cos\phi\tan\theta)r$$
$$\dot{\theta} = (\cos\phi)q - (\sin\phi)r \tag{5.4}$$
$$\dot{\psi} = \frac{\sin\phi}{\cos\theta}q + \frac{\cos\phi}{\cos\theta}r$$

$$\dot{h} = u\sin\theta - v\cos\theta\sin\phi - w\cos\theta\cos\phi \tag{5.5}$$

With known angular rates and linear accelerations in regards to Euler angles it is possible to integrate equations (5.2), (5.4) and (5.5), thus providing fully defined state

vector (5.6). Integration is done with *ode45*, a *MATLAB* function based on explicit *Runge-Kutta* $(4, 5)$ formula.

$$\Delta x = [u, v, w, \phi, \theta, \psi, h] \tag{5.6}$$

From known variables of state vector it is simple to derive other variables: angle of attack α, angle of sideslip β and true airspeed TAS, (5.7).

$$\begin{aligned}
\alpha &= \tan^{-1}(w/u) \\
\beta &= \sin^{-1}(v/TAS) \\
TAS &= \sqrt{u^2 + v^2 + w^2}
\end{aligned} \tag{5.7}$$

It is necessary to state that expression used to calculate angle of sideslip in equations of motion *MATLAB* script differs from cited literature. Angle defined in (5.8) is the horizontal angle of aerodynamic velocity vector.

$$\beta = \tan^{-1}(v/u) \tag{5.8}$$

5.2. FPR method

With kinematic equations providing a state vector, other states can be derived, namely true airspeed, dynamic pressure, angle of attack and angle of sideslip. These derived states are compared with the measured values and when a systematic error in data is present an error model can be developed. Each of the sensor error model contains several parameters, like bias, slope and so on. There are two methods for doing FPR, one being extended Kalman filter having a stochastic nature, which is more accurate but also more complex. Simpler method used for many practical cases is called output-error method, having a deterministic nature.

5.2.1. Output-Error Method

In this case, Output-Error Method (OEM) was used and it will be briefly explained following Figure 5.1.

Dynamic System represents aircraft motion which for a given input has noisy measured response z. This response is then compared with computed system response derived from system error models, y. Parameters used in sensor error model are then optimized

with the goal of minimizing response error $e = (z - y)$.

In depth method description is found in [5].
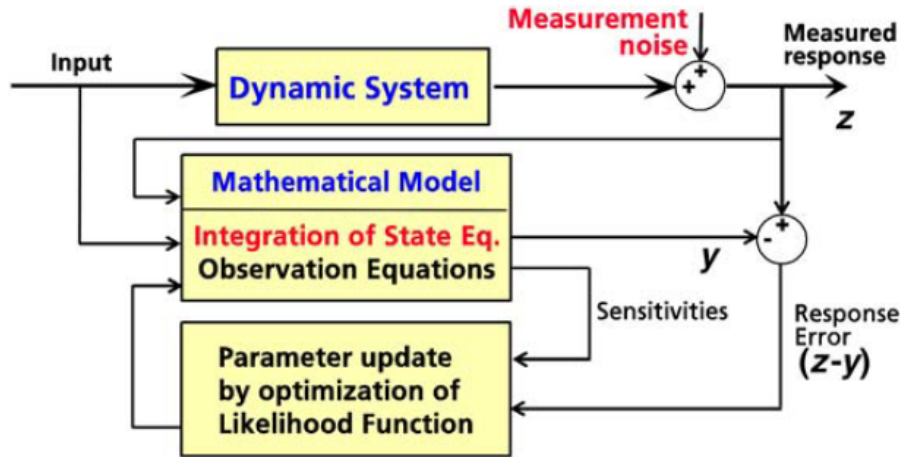
Figure 5.1: Output-Error Method Scheme [5]

5.3.   Reconstruction Process

The whole process of reconstructing flight trajectory is iterative and a script called *Fitlab* is used. Script allows easy adjustment of error models, so it is straightforward to use and can be applied to different airplane configurations. Output of the script shows cost of the function and correlation between parameters. Cost of the function needs to be minimized with each iteration, so that the result is converging. If the correlation is higher than |0.90| the script will show a warning. More about *Fitlab* reader can find in [9].

Even though IMU is more accurate, due to previously stated misalignment it was decided, in [3], to reconstruct sensor error models to match quantities measured by ADB.

Manoeuvres used in FPR:

- Stall

- Steady Heading Steady Sideslip (SHSS)

- Phugoid

- Short Period

- Dutch Roll

- Spiral Check

- Bank to Bank Roll

Iterative procedure shown in 5.2 is simple, yet time exhausting. In the first step parameters for selected stall manoeuvres are estimated. With those parameters set, next step is to select only SHSS manoeuvres and run the process without iteration in order to see how good sensor error model is when applied to another manoeuvre. After that the error model is expanded if there is a need for it and added parameters are estimated. Then the model is returned to stall manoeuvres and ran again, to see how good of a fit it is. If the fit is adequate, phugoid and spiral check manoeuvres come next. Same as before, the error model is expanded if there is a need for it and added parameters are estimated once again, then the model is returned to stall manoeuvres to check differences between measured and reconstructed signals. As it is intuitive, the process is continued for all manoeuvres and returned to stall until the sensor error model is good enough.

The procedure is done for one state at a time and then the whole process is repeated for another state, e.g. first for α, then β and so on.
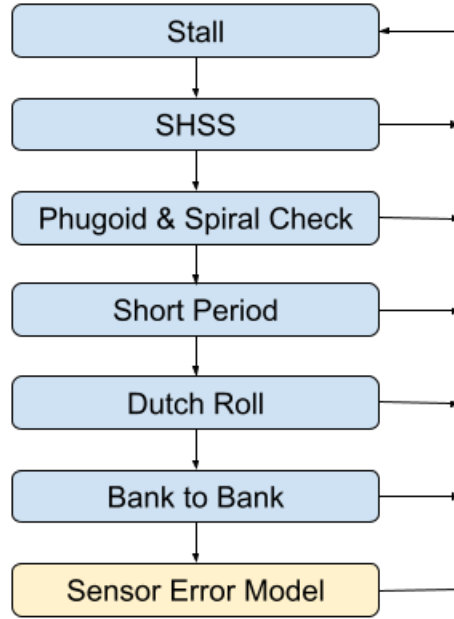
Figure 5.2: Iteration procedure scheme

5.3.1.   Dynamic pressure error model

True airspeed model is not explicitly defined, but rather through Mach number. This way the effect of compressibility is taken into account. It is better said that this is dynamic pressure error model rather than TAS model.

$$M = \frac{TAS}{c}$$
$$q_c = p_s \left[(1 + 0.2M^2)^{7/2} - 1\right] \tag{5.9}$$

Where c is ambient speed of sound with γ being isentropic expansion factor, R specific gas constant of air and T ambient temperature. Dynamic pressure q_c is calculated from measured static pressure p_s.

$$c = \sqrt{\gamma R T} \tag{5.10}$$

Dynamic pressure error model is presented in equation (5.11), parameters values are shown in Table 5.1.

$$q_{c,recon} = b_{q_c} + k_{q_c} q_c + k_{q_c,\beta} |\beta| \tag{5.11}$$

Table 5.1: Dynamic pressure error model parameters

Parameter	Value	Unit	Meaning
b_{q_c}	-96.292	Pa	Dynamic pressure bias
k_{q_c}	1.09037	-	Dynamic pressure slope
$k_{q_c,\beta}$	$-3.45324 \cdot 10^2$	Pa/rad	AoS dependent dynamic pressure gain

With the reconstructed dynamic pressure, reconstructed true airspeed is obtained going back into equations.

$$M_{recon} = \sqrt{5 \left[\left(\frac{q_{c,recon}}{p_s} + 1 \right)^{2/7} - 1 \right]} \tag{5.12}$$

$$TAS_{recon} = M_{recon} \cdot c \tag{5.13}$$

5.3.2.   Angle of Attack error model

Unlike true airspeed, the angle of attack error model is written out explicitly:

$$\alpha_{recon} = b_\alpha + k_\alpha \alpha + k_{\alpha,TAS}|TAS - TAS_\alpha| + k_{\alpha,\beta}|\beta| \tag{5.14}$$

with values presented in Table 5.2.

Table 5.2: Angle of attack error model parameters

Parameter	Value	Unit	Meaning
b_α	-0.119268	rad	Angle of attack bias
k_α	1.75584	-	Angle of attack slope
$k_{\alpha,TAS}$	$4.84644 \cdot 10^{-3}$	$(\text{rad} \cdot \text{s})/\text{m}$	TAS dependent angle of attack gain
$k_{\alpha,\beta}$	-0.249225	-	Angle of sideslip dependent angle of attack gain

At some point iteration seemed not to improve, so additional plots were made in order to get better dependency to parameters. A plot in which AoA residuals are plotted versus true airspeed is shown in Figure 5.3. From this plot, using $MATLAB$ data statistics, mean value of TAS is obtained and it is equal to 46.25 m/s.
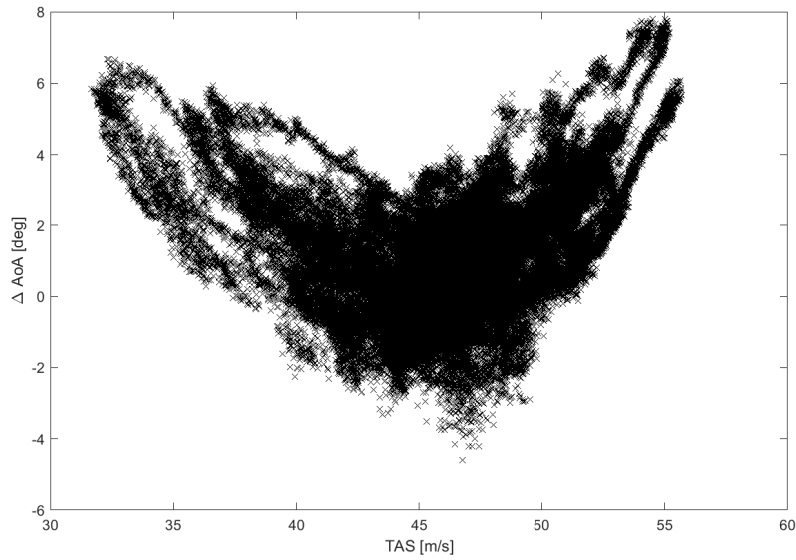
Figure 5.3: Residual plot of α vs TAS

Figure 5.4 shows relation of reconstructed angle of attack with regards to "ideal" 45°
angle line where α_{recon} would be the same as α. Noted that for this case $TAS = 46.25$
m/s and $\beta = 0°$. At point T reconstructed angle of attack line intersects with the
"ideal", meaning that for that value measured and reconstructed value are the same.
It can be seen that below point T reconstruction underestimates the value while above
point T it overestimates.
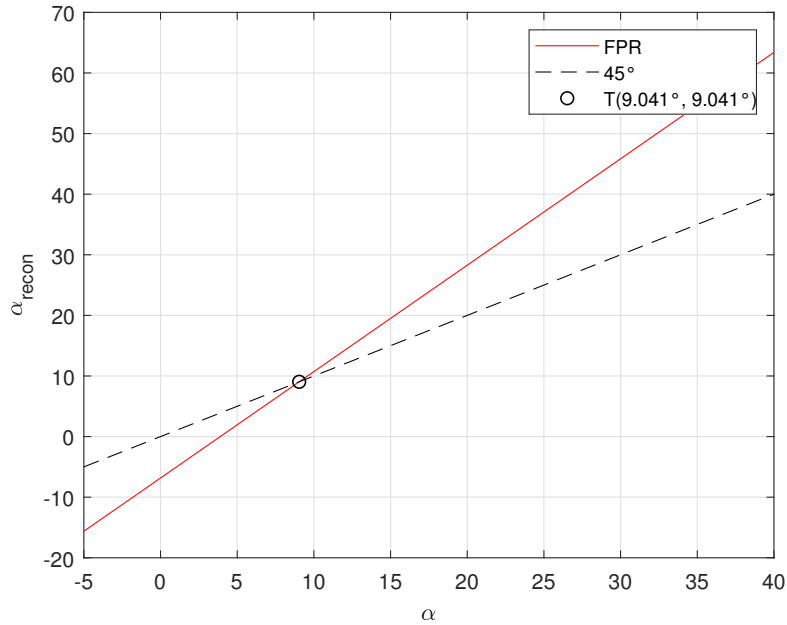
Figure 5.4: Reconstructed α in regards to "ideal"

5.3.3.   Angle of Sideslip error model

As well as error model above, this one can also be explicitly written out. Although simple, error model provides reasonable fit. Values for the error model are found in Table 5.3.

$$\beta_{recon} = b_\beta + k_\beta \beta \tag{5.15}$$

Table 5.3: Angle of sideslip error model parameters

Parameter	Value	Unit	Meaning
b_β	$-8.0641 \cdot 10^{-3}$	rad	Angle of sideslip bias
k_β	0.984573	-	Angle of sideslip slope

5.4.   FPR Results

Having multiple manoeuvres in the same plot would reduce the number of plots presented, but due to figures being large the results shown wouldn't be visible. It was decided to separate manoeuvres into low and high dynamic modes in which every manoeuvre will be plotted individually. On each plot five manoeuvres will be shown making sure that the plot isn't overfilled.

In these figures blue line represents measured signal, i.e. measured by ADB, and red line represents reconstructed signal, angles are shown in degrees, airspeed in knots, altitude in meters and on horizontal axis is time in seconds.

5.4.1.   Low Dynamic Modes

Low dynamic mode manoeuvres shown are: stall, phugoid, steady heading steady sideslip and spiral check.

In stall manoeuvres most important is to fit the decreasing airspeed and increase of the angle of attack, given that the range of AoA is large covering big part of the flight envelope. In Figure 5.5 measured and reconstructed line coincide reasonably well during the whole manoeuvre, except when the true airspeed enters the area surrounding the curves lowest point, that is when AoA curve comes close to the highest point of the curve. In that part values enter nonlinear area, so for that to be adequately modelled it would require nonlinear parameters. Angle of sideslip, although not of upmost importance in this manoeuvre, shows a good fit. In fourth manoeuvre there is a divergence of curves as the absolute value of β increases, but it will be shown in other manoeuvres that for the high values of β reconstructed signal matches the measured. Euler angles show almost perfect fit, residuals of the signals is negligible.
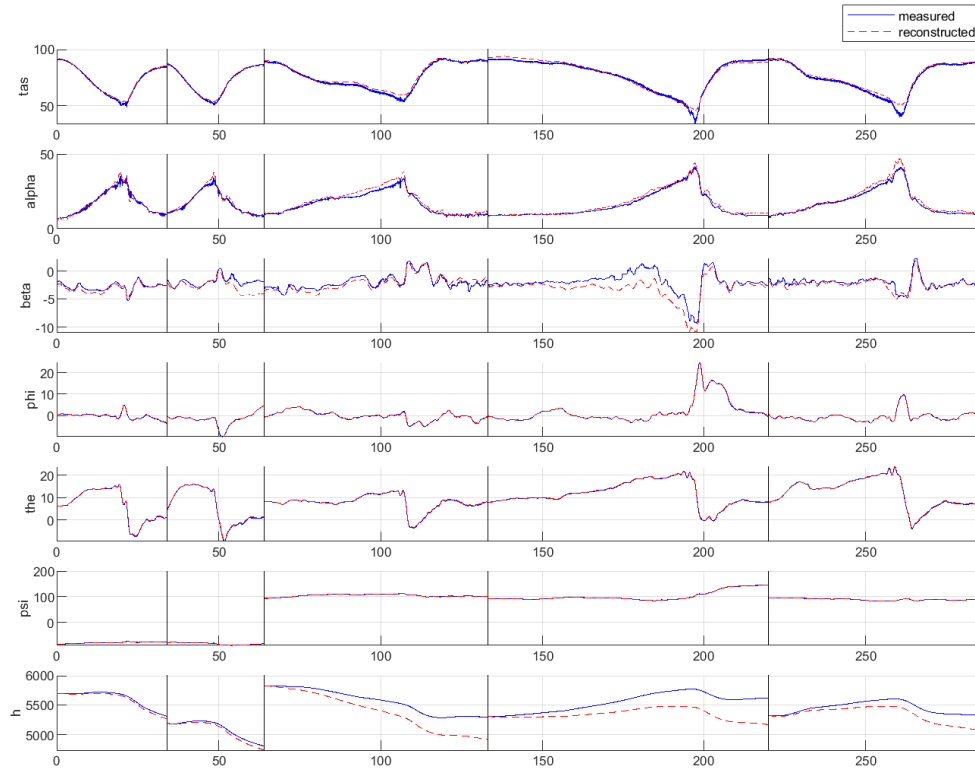
Figure 5.5: FPR results for five stall manoeuvres

Observing Figure 5.6 of phugoid manoeuvres, long duration longitudinal mode, it is visible that TAS curves start to diverge as the end of the manoeuvre approaches. That happens due to cumulative error being imposed in the next step of computation. This issue could be resolved with splitting manoeuvres in two parts. Still the match is more than satisfactory as the reconstructed signal covers high and low amplitudes. Dynamic response of reconstructed AoA value follows the measured signal, not perfect but adequately. It must be noted that the curves matched better when there were quadratic term in error model, e.g.

$$k_{\alpha,TAS^2}(TAS - TAS_\alpha)^2 \tag{5.16}$$

$$k_{\alpha^2}(\alpha - T_\alpha)^2 \tag{5.17}$$

where T_α denotes a threshold value of α.

But including these terms in AoA error model brought major issues when inverting the model. Quadratic term when inverting provides two solutions, one having no physical meaning. Along with that error model was split in three parts, improving the trajectory reconstruction but with said issue it was decided to simplify the error model. Why there is a need for inversion will be discussed later in section 5.5.

AoS matching is reasonable with second and third manoeuvres having the same issue as discussed in stall manoeuvres for Figure 5.5. Again Euler angles signal residuals are negligible.
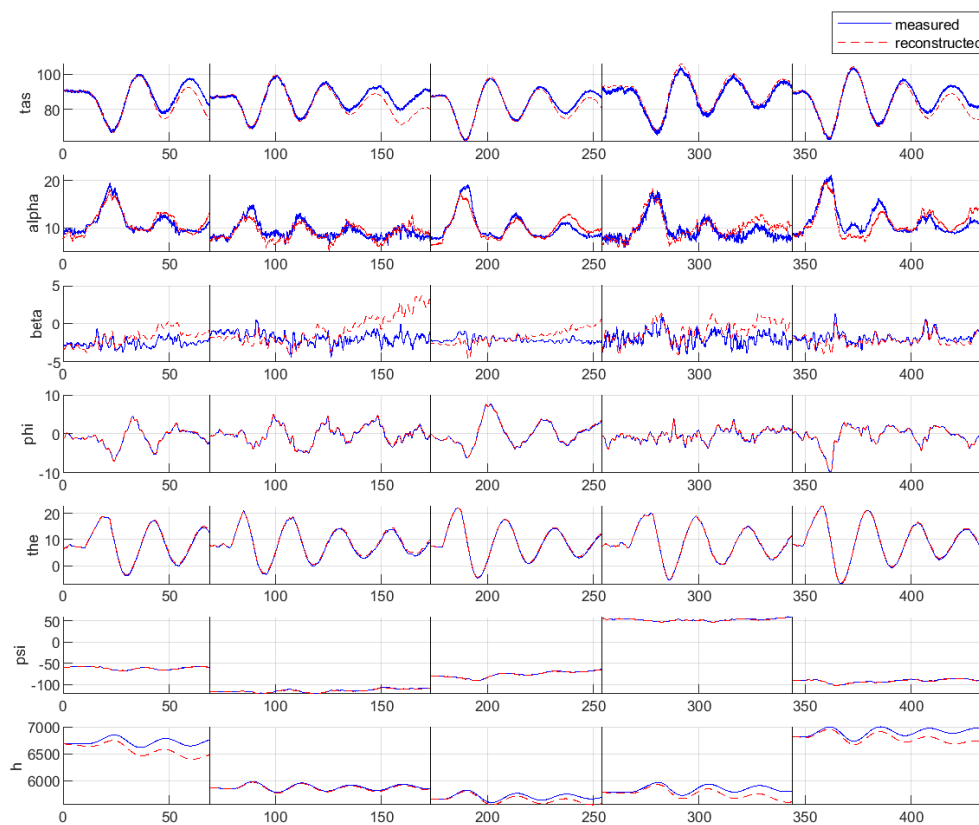
Figure 5.6: FPR results for five phugoid manoeuvres

In SHSS, a lateral mode, most important signal reconstruction is the angle of sideslip. Looking at the Figure 5.7 AoS has a large range from around 20 to -15 degrees and the

dynamic response of the reconstructed signal is suitable ensuring that this part of flight envelope is covered for aerodynamic modelling. Angle of attack signal reconstruction has an issue in the fifth manoeuvre where, from the start, initial value differs. Having that difference affects the whole process of reconstruction, so the reader should be careful when observing that plot. Also, for the same reason as in phugoid manoeuvres, TAS curves approaching the manoeuvre's end begin to differ.
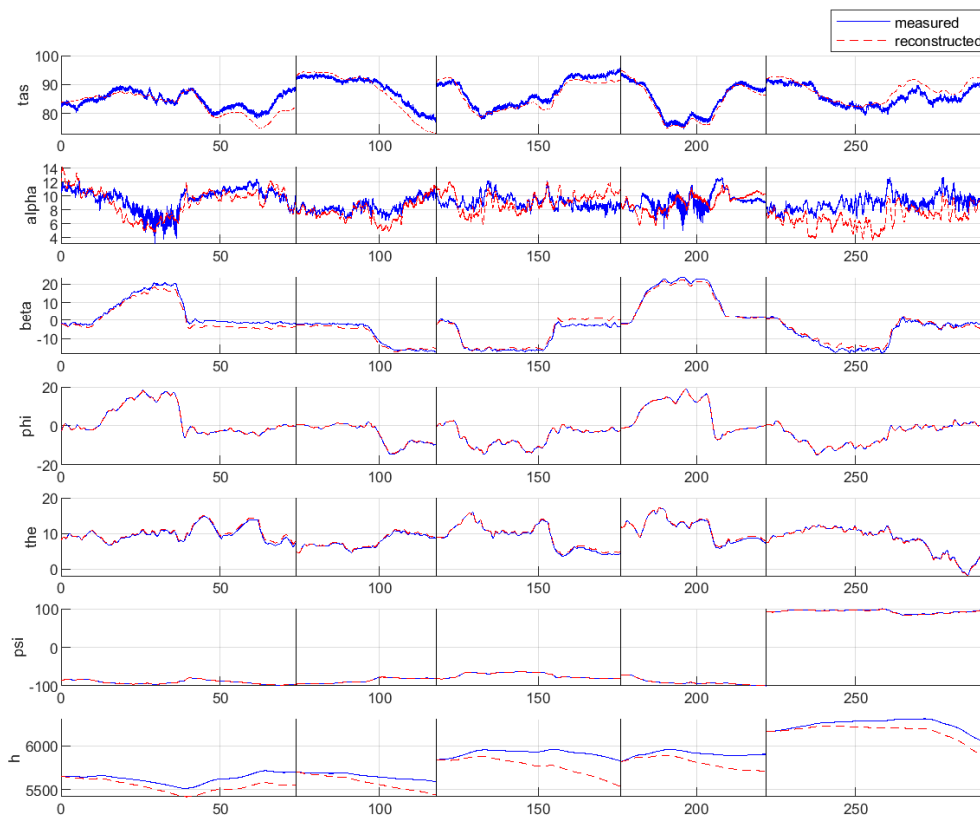
Figure 5.7: FPR results for five steady heading steady sideslip manoeuvres

Unfortunately, not every manoeuvre could be reconstructed equally good. For example, phugoid and SHSS had an advantage in reconstructing over spiral check, due to information one can obtain from them. But, even still, it can be seen in Figure 5.8 that TAS and α signals are reasonable with divergence occurring towards the end of some manoeuvres. β signal on first sight has a big difference in second and third manoeuvre

which would indicate that the error model is not suitable, however in other manoeuvres reconstructed signal matches the measured one quite well. Origin of that problem could be in the measured signal itself, e.g. noise or interference on ADB.
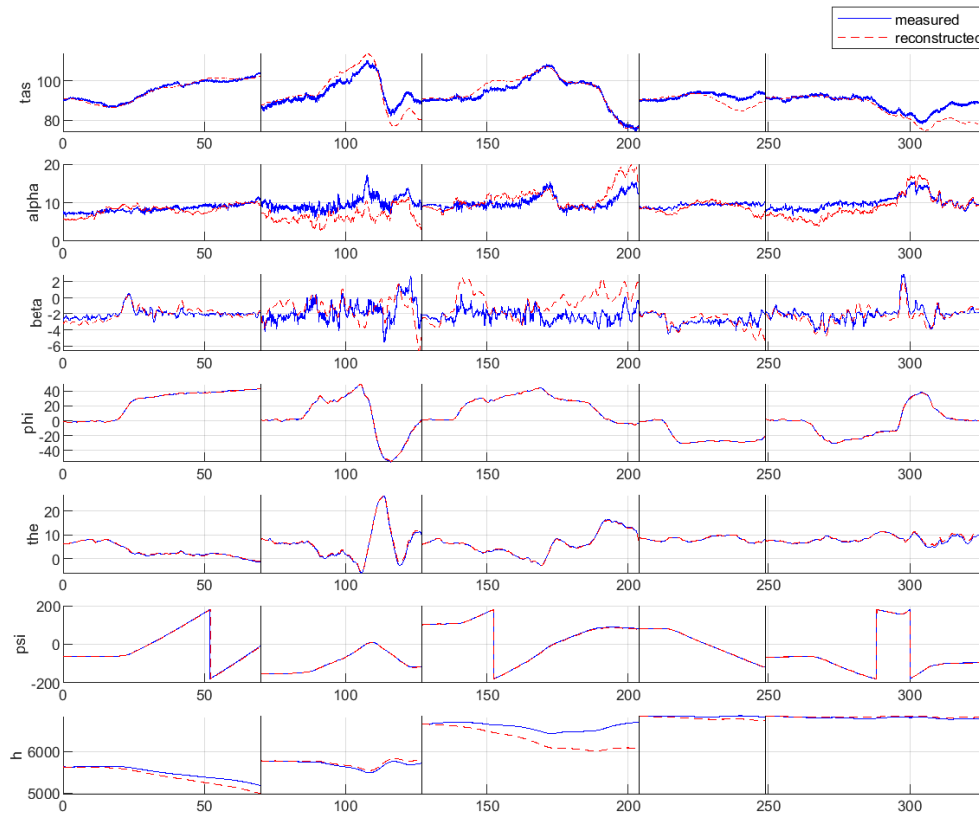
Figure 5.8: FPR results for five spiral check manoeuvres

5.4.2.   High Dynamic Response

High dynamic mode manoeuvres shown are: short period, dutch roll and bank to bank roll.

Short period motion is a fast-responding longitudinal mode from which most information regarding vertical and pitching motion can be obtained. It can be seen from Figure 5.9 that the match of reconstructed signal and measured one is great. Not visible on the figure is that reconstructed AoA overshoots at the peaks.
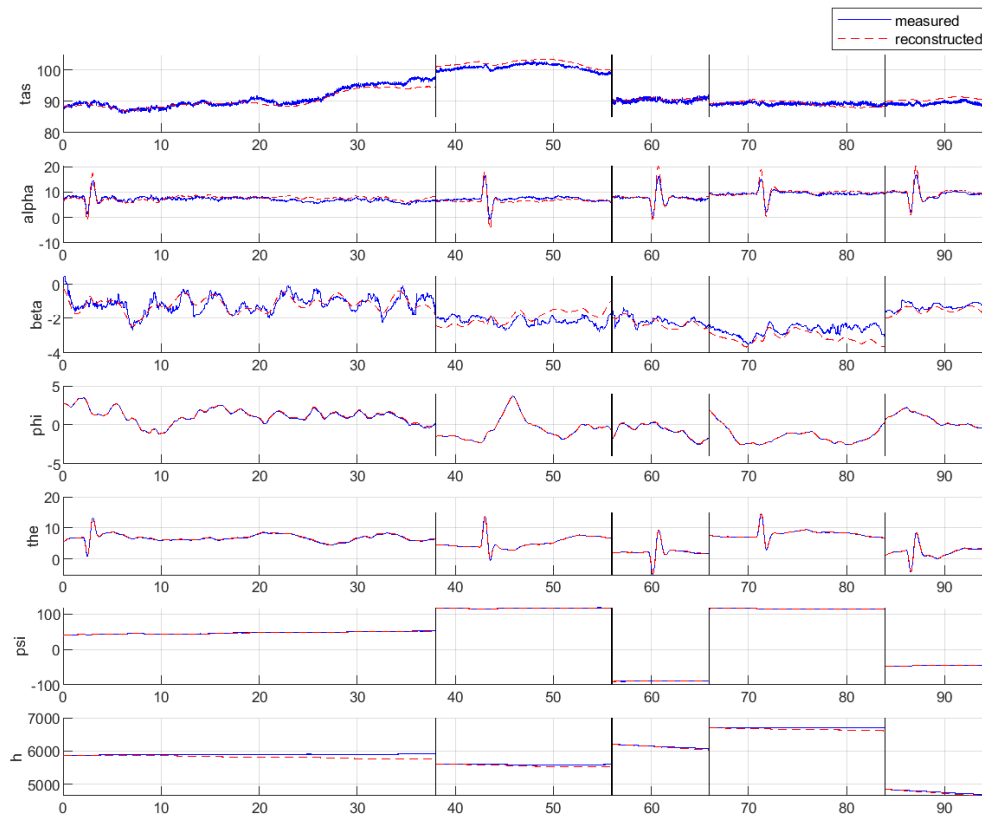
Figure 5.9: FPR results for five short period manoeuvres

To allow estimation of lateral-directional derivatives two manoeuvres are performed, dutch roll and bank to bank. Flight path reconstruction of these manoeuvres are shown in Figures 5.10 and 5.11.
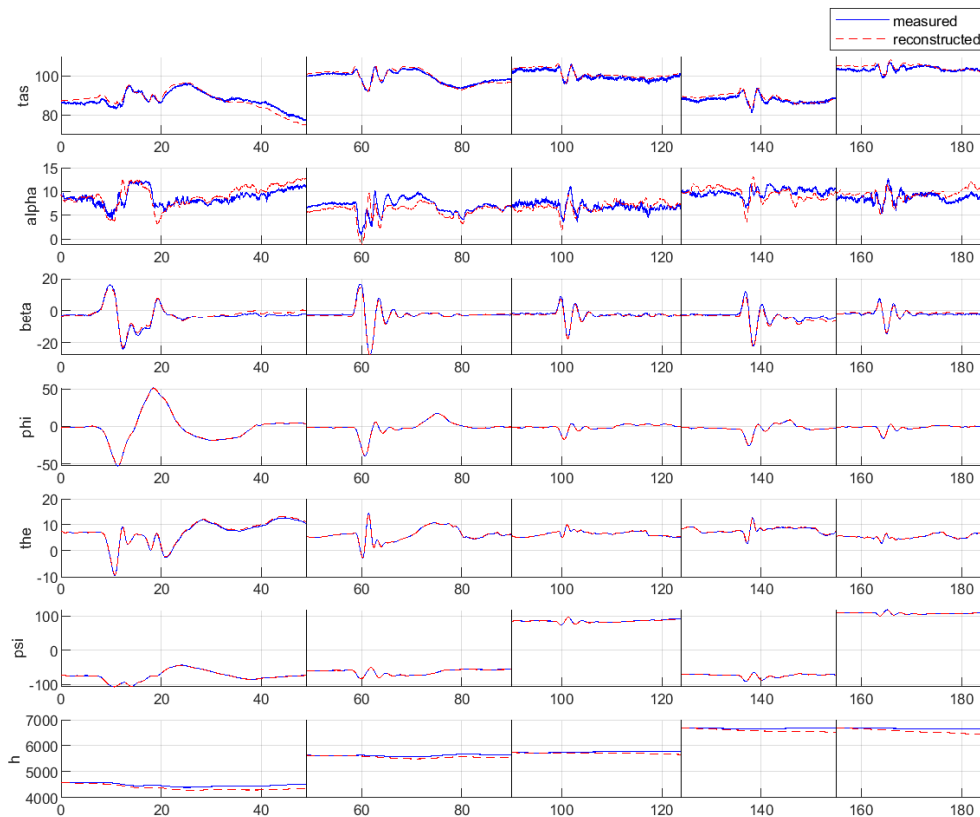
Figure 5.10: FPR results for five dutch roll manoeuvres

Flight path trajectory for dutch roll manoeuvres is reconstructed well, primarily for TAS and AoS. By the end of the first manoeuvre there is a slight drift in true airspeed, resulting from cumulative error. Also reconstructed AoS shows good dynamics, however there is underestimation of positive amplitude peaks. Reconstructed signal of AoA displays dynamics not as close to the measured signal, but it was decided that the matching is adequate since for lateral stability AoS is the key factor.

Reconstructed signals of bank to bank manoeuvres are of reasonable dynamics. The only issue is with AoS in third manoeuvre but, again, that is due to cumulative error, which could be resolved with cutting the manoeuvre at the start of the drift.
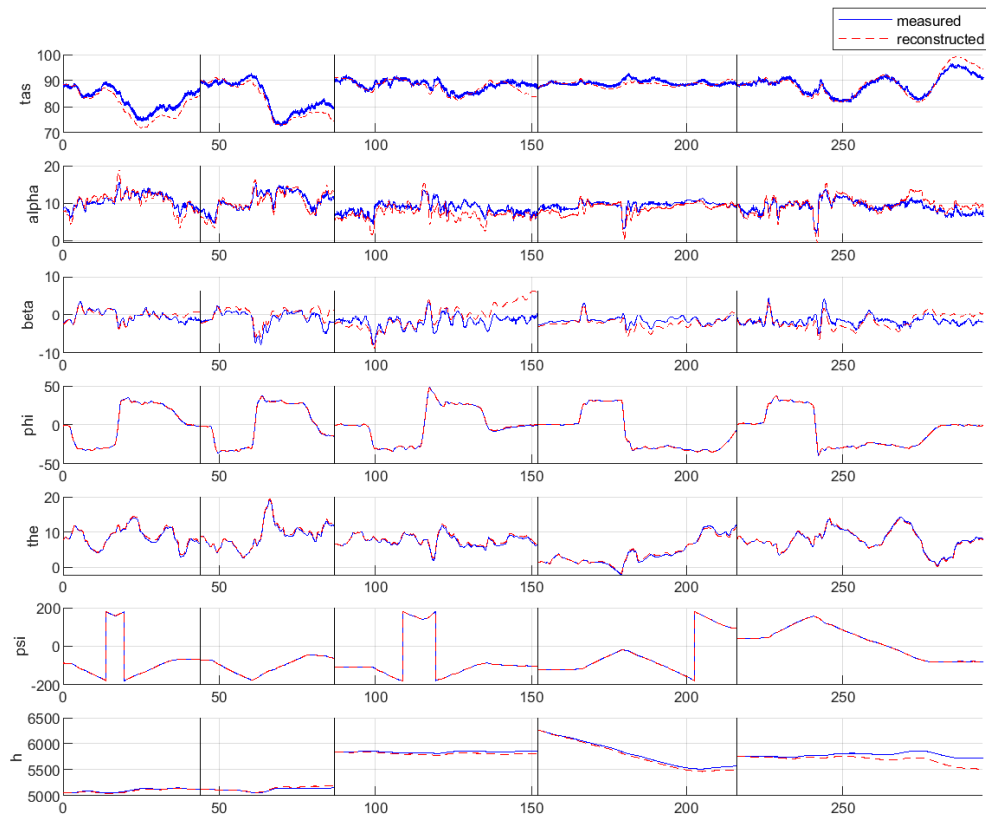
Figure 5.11: FPR results for five bank to bank roll manoeuvres

How a residual plot looks like is shown in Figure 5.12, in which Euler angles residuals are plotted. For two stall, phugoid and short period manoeuvres selected, residuals are relatively small meaning that the reconstruction of these values is good.
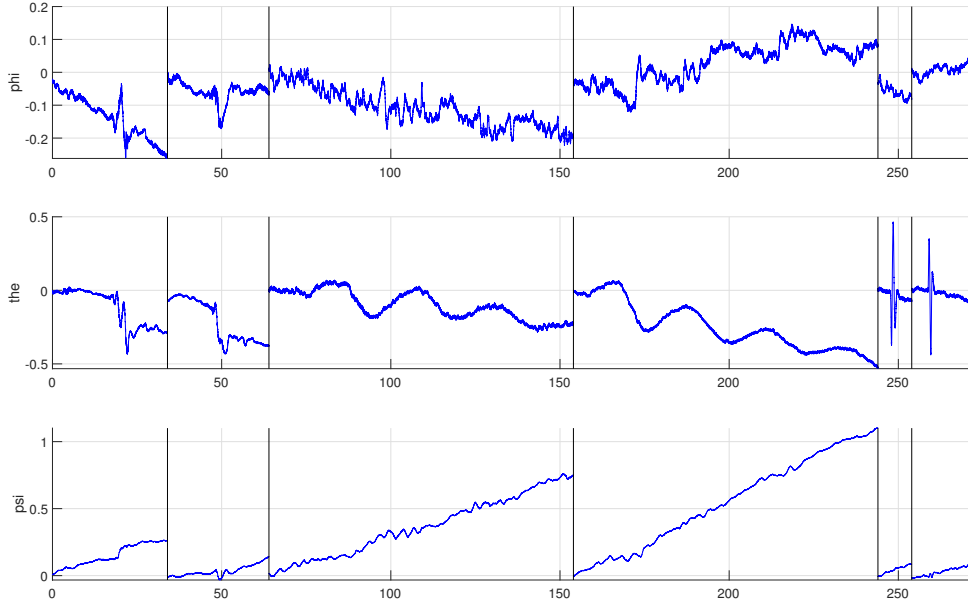
Figure 5.12: Euler angle residuals for two stall, phugoid and short period manoeuvres

5.5.   Inversion

In the FPR, for this project, reconstructed data is corrected to match the measured one. However, it's necessary to correct the measured values to the reconstructed ones. For that reason, inversion of (5.11), (5.14) and (5.15) is done. Error model values of parameters can be found in tables 5.1, 5.2 and 5.3.

$$\beta_{corr} = \frac{\beta_m - b_\beta}{k_\beta} \tag{5.18}$$

$$q_{c,corr} = \frac{q_{c,m} - b_{q_c} - k_{q_c,\beta}|\beta_m|}{k_{q_c}} \tag{5.19}$$

$$\alpha_{corr} = \frac{\alpha_m - b_\alpha - k_{\alpha,TAS}|TAS - TAS_\alpha| - k_{\alpha,\beta}|\beta_{corr}|}{k_\alpha} \tag{5.20}$$

Regarding the issues of inverting error model with quadratic terms, the part that brought more troubles was the three-part curve split. For values in proximity of curve slope change, corrected value behaved unreasonable due to sensitivity caused by the slope. So, again, simpler model was used.

Results of the correction are shown in figures 5.13, including one stall, phugoid, steady heading steady sideslip and spiral check manoeuvres and 5.14, including one short period, dutch roll and bank to bank roll manoeuvres. Measurement units of values shown are the same as in previous plots.

Just a remark, values in these figures do not need to match, rather differences are expected.
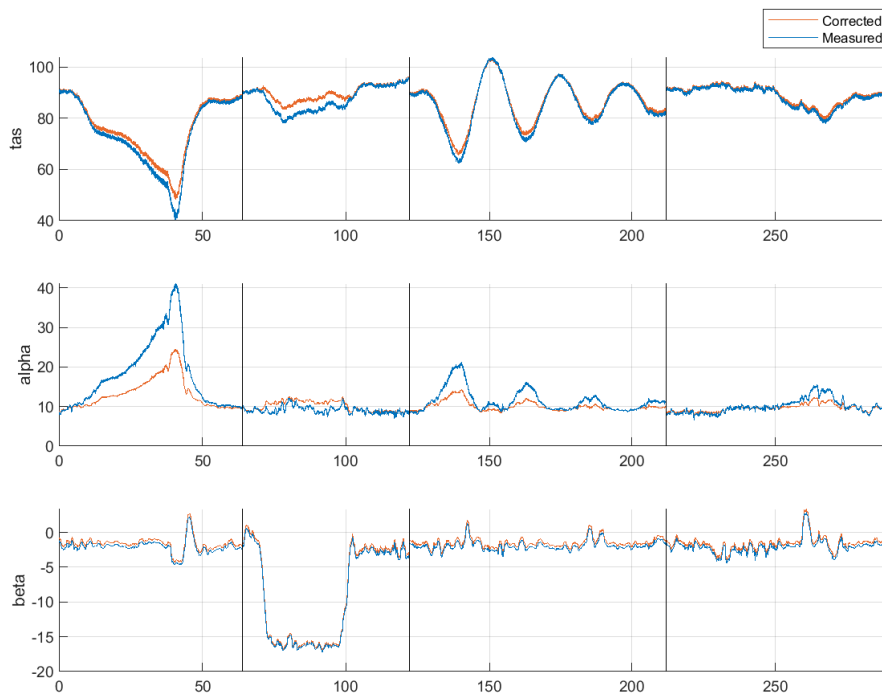
Figure 5.13: Sensor error model correction for low dynamic modes

Correction of measured data will be discussed on the example of stall manoeuvre. Angle at which aircraft stalls is said to be around 20 degrees. Measured α goes way beyond, into values impossible for aircraft to reach in controlled flight.
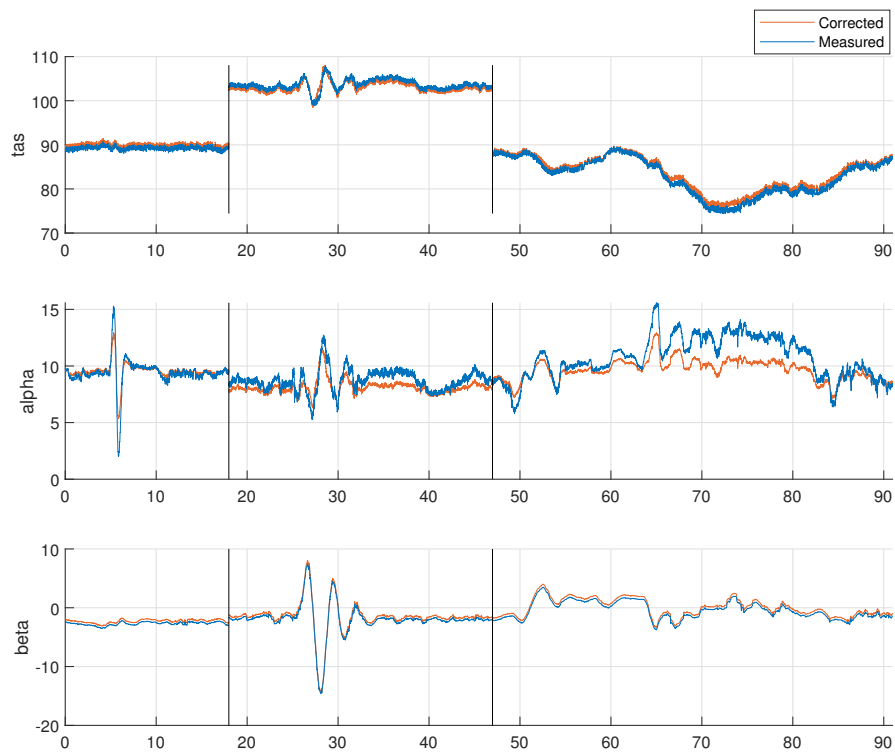
Figure 5.14: Sensor error model correction for high dynamic modes

All the scripts and functions used are found in A.3..

6 | Parameter Estimation

To understand how parameters are estimated, reader will be shown a short summary of linear regression in section 6.2. But before that, aerodynamic coefficients need to be determined.

6.1. Aerodynamic Coefficients

In practice aerodynamic coefficients are more often used instead of components of aerodynamic forces and moments. Since they are not directly measured, they need to be derived. These terms come from already discussed equations of motions found in section 5.1., [8]. Rewriting equation (5.3) so that aerodynamic forces are shown on the left side of the equation leads to:

$$\mathbf{F}_{aero} = m\mathbf{a} - \mathbf{T}$$

$$\begin{bmatrix} X \\ Y \\ Z \end{bmatrix} = m \begin{bmatrix} a_x \\ a_y \\ a_z \end{bmatrix} - \begin{bmatrix} T\cos\alpha_T \\ 0 \\ T\cos\alpha_T \end{bmatrix}. \tag{6.1}$$

Coefficients are non-dimensional values which arrive from division of aerodynamic forces and moments with reference force and moment. Reference force is the product of reference pressure q, and area S_{ref}, with reference moment being the product of reference force and reference length.

Reference pressure is dynamic pressure calculated with true airspeed and is always the same.

$$q = \frac{\rho V^2}{2} \tag{6.2}$$

Aerodynamic force coefficients are presented in table 6.1.

Table 6.1: Aerodynamic force coefficients

Axial force coefficient	$C_X = \dfrac{X}{qS_{ref}}$
Lateral force coefficient	$C_Y = \dfrac{Y}{qS_{ref}}$
Normal force coefficient	$C_Z = \dfrac{Z}{qS_{ref}}$

Even though the standards state that the airplane has one reference length, in practice there are two. For roll and yaw that is wingspan b and for pitching that is mean aerodynamic chord $\bar{c}$.

Table 6.2: Aerodynamic moment coefficients

Roll coefficient	$C_l = \dfrac{L}{qS_{ref}b}$
Pitch coefficient	$C_m = \dfrac{M}{qS_{ref}\bar{c}}$
Yaw coefficient	$C_n = \dfrac{N}{qS_{ref}b}$

When determining aircraft performance, aerodynamic coefficients in aerodynamical coordinate system are used, C_D and C_L. Relation between these coefficients is shown in (6.3).

$$
\begin{aligned}
C_D &= -C_X \cos\alpha \cos\beta - C_Y \sin\beta - C_Z \sin\alpha \cos\beta \\
C_L &= C_X \sin\alpha - C_Z \cos\alpha
\end{aligned} \tag{6.3}
$$

For modelling thrust coefficient has also been used. It comes from expression (6.4).

$$C_T = \frac{T \cos\alpha_T}{qS_{ref}} \tag{6.4}$$

Aerodynamic moments that refer to the aerodynamic reference point are mainly used. Transformation of aerodynamic moments from the CG to the reference is shown in [3].

These aerodynamic coefficients are compared to the ones obtained from parameter estimation.

6.2.   Liner Regression

Regression techniques describe the relations between *explanatory* or *predictor* variables and a variable of specific interest, known as *response* or *target* variable. That can be mathematically presented as:

$$y \approx f(x_1, x_2, ..., x_p). \tag{6.5}$$

Predictor variables, or just predictors, are $(x_1, x_2, ..., x_p)$, p being the number of predictors. The goal is to identify function f which defines how said predictors need to be combined to get specified response y. Most common type of regression is *linear regression model*.

$$y = \beta_0 + \beta_1 x_1 + \beta_2 x_2 + ... + \beta_p x_p \tag{6.6}$$

From observed data set it is necessary to determine parameters $(\beta_1 + \beta_2 + ... + \beta_p)$ in a process called *estimation.*
Important thing to note is that only the parameters, but not the predictors, need to be linear in the model. For example, model shown in (6.7) is still linear.

$$y = \beta_0 + \beta_1 x_1 + \beta_2 (x_1)^2 + \beta_3 log(x_2) + \beta_4 x_1 x_2 + E \tag{6.7}$$

E is a mean zero random error, which stands for deviation of estimated specific value from the actual value, i.e. imperfection.

Or, in this case where the interest is aerodynamic modelling from flight test data, example structure shown in (6.8) is still linear.

$$C_m = C_{m,0} + C_{m,\alpha}\alpha + C_{m,\alpha^3}\alpha^3 + C_{m,q}q^* + C_{m,\delta_e}\delta_e + C_{m,\delta_e}\delta_e^3 \tag{6.8}$$

6.2.1.   Ordinary Least Squares

One of the most commonly used algorithm is the ordinary least squares (OLS), also used for this thesis. In OLS the goal is to minimize the sum of squared differences r_i of the observed values y_i and computed values $\hat{y}_i$. That means that for every data point, for each time increment, difference between the actual and estimated value is to be minimal.

$$\sum_{i=1}^{n} r_i^2 = \sum_{i=1}^{n}(y_i - \hat{y}_i)^2 = \min \tag{6.9}$$

This subsection and whole section of linear regression 6.2. is based on [10].

6.3.   Model development summary

When modelling each aerodynamic coefficient individually one has to be wise with the selection of manoeuvres. Not every manoeuvre is suitable to excite desired dynamic for specific coefficient. For example, if a current interest lies in lift coefficient a bank to bank manoeuvre will not provide quality data of AoA, but a manoeuvre with a high AoA range, e.g. stall, affects the model in higher scale.

A perfect model would be the same for all manoeuvres, i.e. whole flight envelope, but of course that is more than often not possible. Developed models with estimated parameters cover certain part of the flight envelope and when examining them that should be kept in mind. Another thing is that models which do not include specific parameters cannot replicate aircraft dynamics in manoeuvres where those parameters have influence.

Introduced OLS algorithm with the corresponding function used in modelling has a feature giving more weight the higher the number of observations there are. As all of the manoeuvres in this project have the same increment for observations, longer manoeuvres influence the model more than shorter one, e.g. a phugoid manoeuvre with a $t \approx 60$ s duration receives more weight than a short period with 1/10th of that duration. To counter this when modelling, if a case includes both manoeuvre types, for each long duration manoeuvre included there are several shorter ones.

To avoid this issue another function of linear regression was used, called *fitlm*. This is a *MATLAB* function with a feature to specify a weight vector allowing user to put custom weights to observations, in this case giving more weight to shorter manoeuvres

and thus balancing out manoeuvres selected for model development.

Following section shows developed models and as it will be seen they are not perfect, but for this thesis they are of sufficient accuracy. Limited magnitude of accuracy was set within the framework of this thesis, leaving room for improvement in future work.

Basis of models were set in [3]. All the scripts and functions used are found in A.4.

6.4. Longitudinal motion coefficients

In the framework of this thesis focus was set on longitudinal motion coefficients. They are lift coefficient C_L, pitching moment coefficient C_m and drag coefficient C_D. In the developed model diagrams red colour represents the model, blue colour the actual value and vertical green lines are manoeuvre separators.

6.4.1. Pitching moment coefficient

To excite dynamics of pitching moment, short period and stall manoeuvres were selected. In short period damping effects of oscillation are present to put the aircraft back in steady flight. When high values of AoA occur, for example in a stall manoeuvre, a stable aircraft by default returns to steady flight with nose down motion, decreasing the AoA. Model is shown by equation (6.10). Besides obvious angle of attack α, pitch rate q and elevator deflection δ_e model contains influence of thrust.

$$C_m = C_{m_0} + C_{m,\alpha}\alpha + C_{m,q}q^* + C_{m,\delta_e}\delta_e + C_{m,C_T}C_T \qquad (6.10)$$

Matching of the actual value of the coefficient with the estimated value presents how good the developed model is, Figure 6.1. Plot consists of seven short period manoeuvres and five stalls. As it can be seen for short periods, model does not reach the amplitude peaks, suggesting that a certain effect is not represented by model. Stall matching is satisfactory as model follows the increase of the coefficient. In Figure 6.2 short period manoeuvres are enhanced for better examination. A word of caution for non-linearity area, this model does not include non-linear predictors so the model cannot represent effects there. Parameters estimated with this model are found in table 6.3.
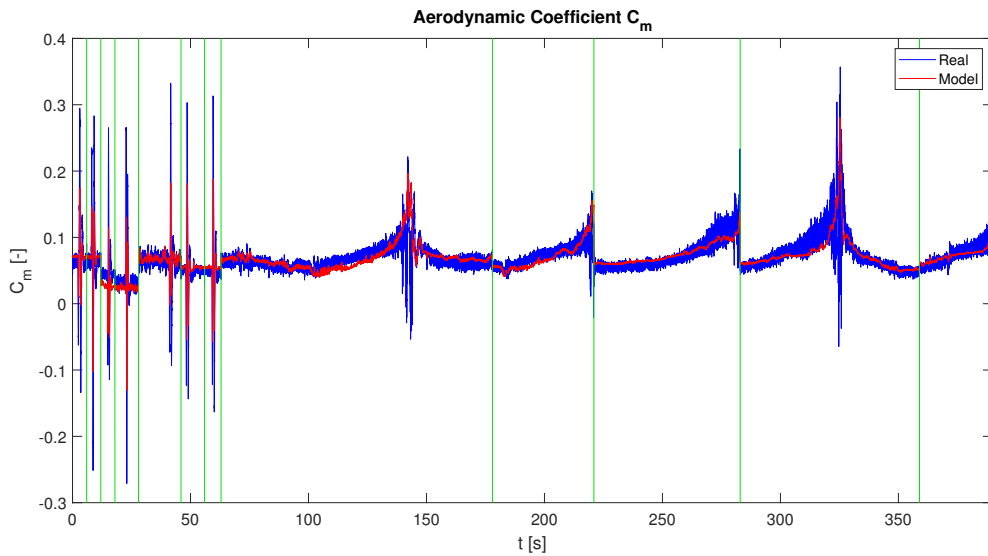
Figure 6.1: C_m model for span of short period and stall manoeuvres

Table 6.3: C_m estimated parameters

Parameter	Value	Unit	Relative error [%]
C_{m_0}	0.089352	–	0.66
$C_{m,\alpha}$	−0.47574	1/rad	0.96
$C_{m,q}$	−5.6724	–	1.69
C_{m,δ_e}	−1.2083	1/rad	0.59
C_{m,C_T}	0.22541	–	0.73

Zero lift pitching moment coefficient is positive, as it is for all stable airplanes, pushing airplane nose up. Another condition of stability, that is satisfied here, is negative value of pitching moment for increasing angle of attack. For positive pitch rate, nose up, elevator deflection is negative, consequently both of these pitching moment derivatives are negative. For airplanes with engines located at the nose, increasing thrust leads to pitching up, therefore there has to be positive pitching moment derivative of thrust coefficient. All parameter values are reasonable, within expected range and relative error for all parameters is quite small.
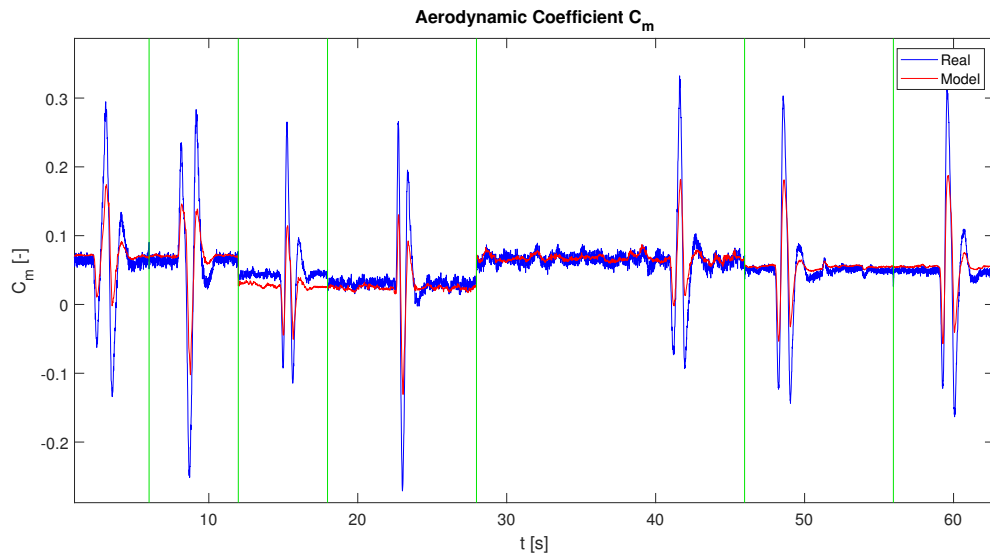
Figure 6.2: C_m model, short period manoeuvres

Visualizing distribution of predictors with histograms allow for detection of skewness in variables, which is a measure of symmetry or better stated lack of it. Normal distribution is desired for better model estimation. As it can be seen from the Figure 6.3 q^* is highly concentrated around zero, AoA is right-skewed and elevator deflection is left-skewed. This could be addressed with variable transformation, but it was not pursued within the framework of this thesis.
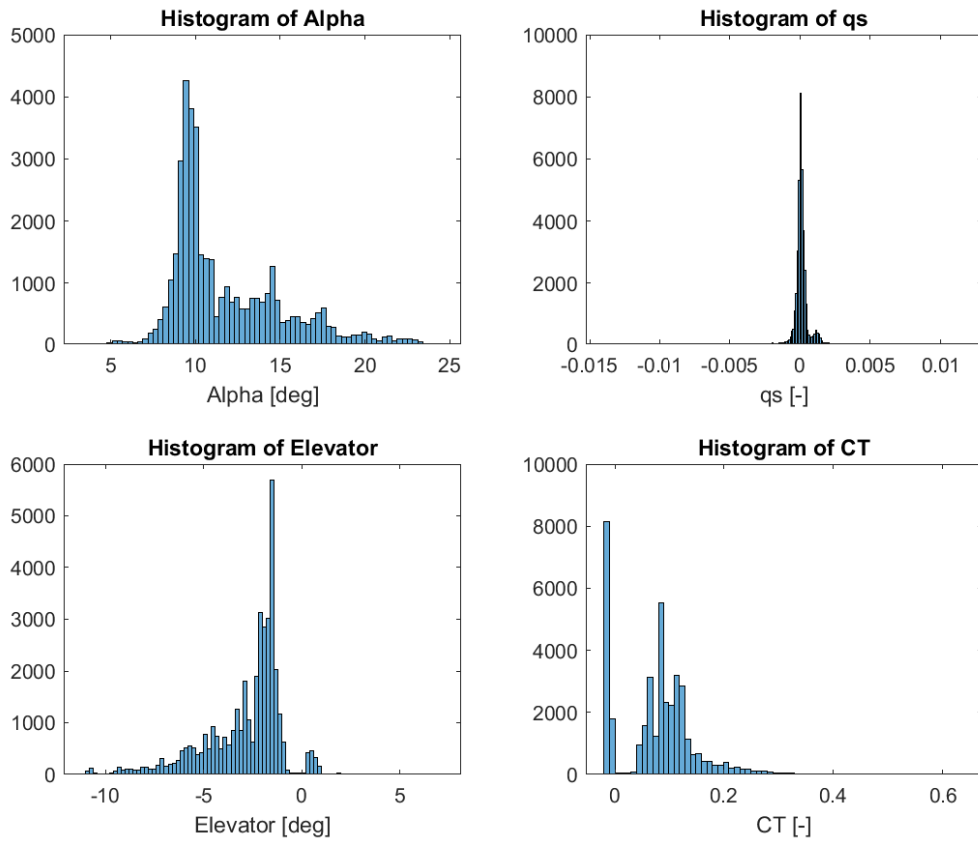
Figure 6.3: C_m predictors histogram

Another way of detecting if an effect is not included in the model is residual analysis, where residuals of response variable, in this case the observed aerodynamic coefficient, are graphically showed versus covariates, that is the predictors. Examining the residual plots one can detect a pattern and thus improve regression. The residual plot of pitching moment coefficient is shown in Figure 6.4:
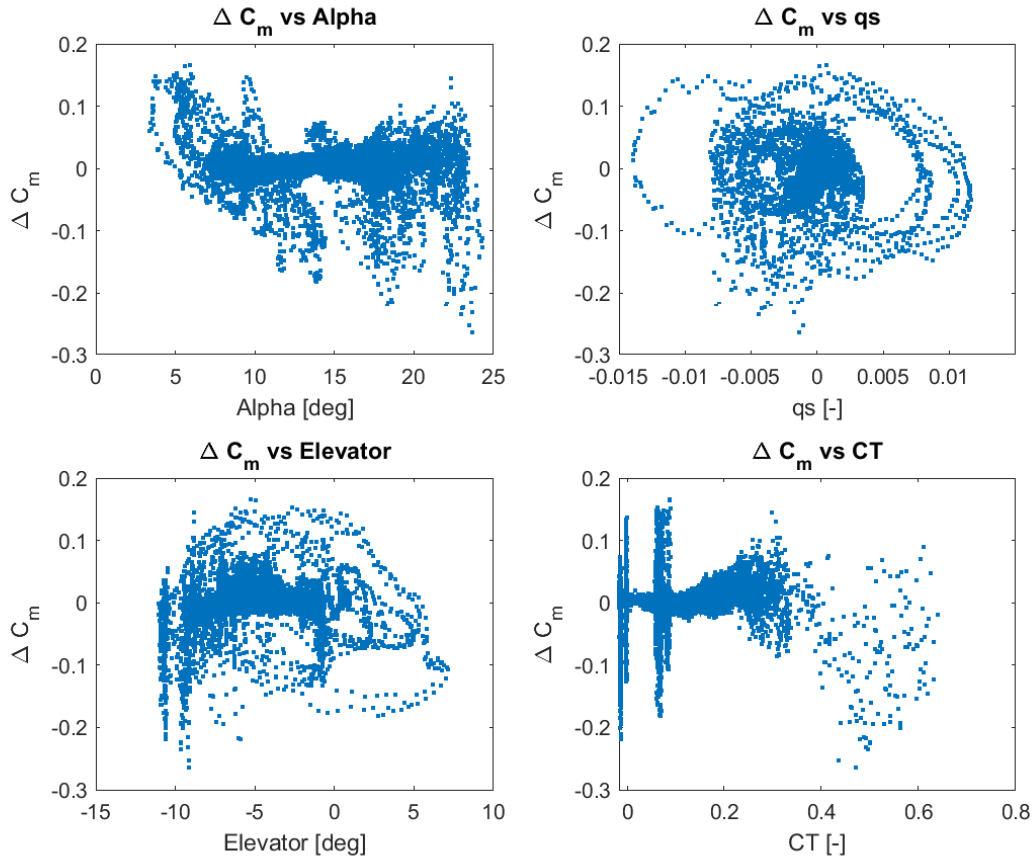
Figure 6.4: C_m residuals versus predictor variables

A pattern is spotted in C_m residuals versus two predictors, AoA and δ_e. A useful tool for fitting included in *MATLAB* was used. Both graphs were satisfactory fitted with cubic curve so higher order polynomial wasn't used, as a result the model is expanded and the parameter results are shown in table 6.5

$$C_m = C_{m_0} + C_{m,\alpha}\alpha + C_{m,q}q^* + C_{m,\delta_e}\delta_e + C_{m,C_T}C_T + C_{m,\alpha^3}\alpha^3 + C_{m,\delta_e^3}\delta_e^3 \qquad (6.11)$$

Table 6.4: C_m expanded model estimated parameters

Parameter	Value	Unit	Relative error [%]
C_{m_0}	0.13369	–	0.82
$C_{m,\alpha}$	-0.87676	1/rad	0.90
$C_{m,q}$	-6.9322	–	1.29
C_{m,δ_e}	-1.8063	1/rad	0.49
C_{m,C_T}	0.20154	–	0.83
C_{m,α^3}	1.7476	$1/\text{rad}^3$	2.26
C_{m,δ_e^3}	24.021	$1/\text{rad}^3$	1.00

With this model, matching with the actual value is better, Figure 6.5, but the model still does not reach amplitude peaks. Also, the offset in the third manoeuvre increases. Since the base model also had offset it is assumed that the expanded one emphasized the error, resulting in bigger offset. A possible reason for that is the absence $\dot{\alpha}$ coefficient derivative, for which article [11] should be studied.
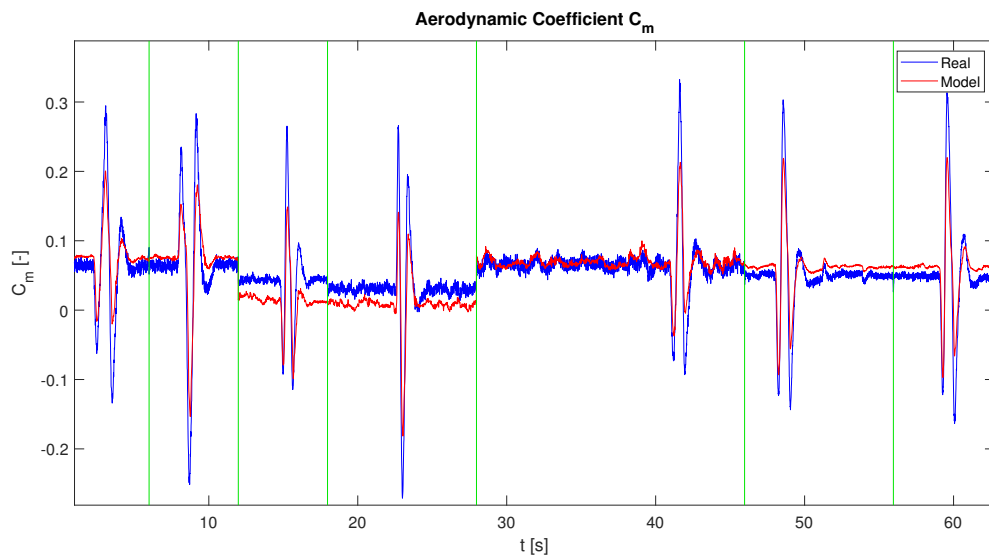
Figure 6.5: C_m expanded model, short period manoeuvres

For the expanded model, functions of covariates are shown on Figure 6.6. Functions of the covariates are expressed in (6.12). It can be seen that pitching moment functions of

normalized pitch rate and thrust coefficient change linearly. Downward slope is present when normalized pitch rate increases, which is a desired effect. Increase of thrust results in upward pitching motion. Given that the engine is located at the nose of the aircraft this effect was predicted. Pitching moment functions of AoA and elevator deflections are defined as cubic splines. For high angle of attack, as stated before, stable aircraft will pitch down. Referring to defined conventions in section 3.2., for negative elevator there is positive pitching moment, i.e. pitching moment coefficient. The function follows that conventions as it can be seen that the pitching moment is negative when elevator deflection value is positive.

$$
\begin{aligned}
C_m(\alpha) &= C_{m,\alpha}\alpha + C_{m,\alpha^3}\alpha^3 \\
C_m(q) &= C_{m,q}q^* \\
C_m(\delta_e) &= C_{m,\delta_e}\delta_e + C_{m,\delta_e^3}\delta_e^3 \\
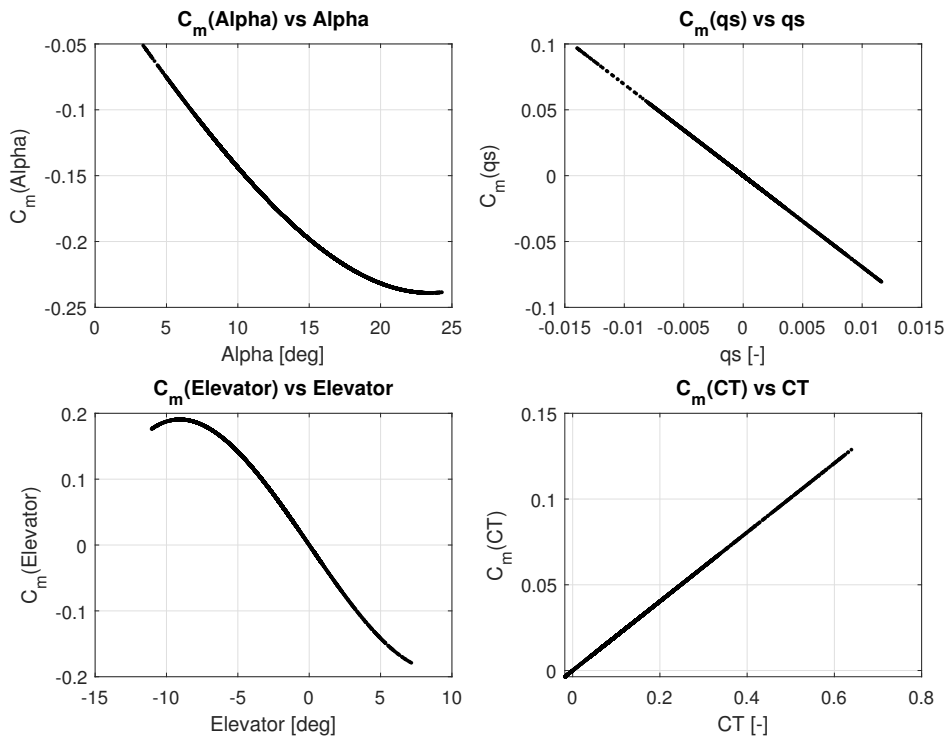C_m(C_T) &= C_{m,C_T}C_T
\end{aligned}
\tag{6.12}
$$

Figure 6.6: C_m predictors functions

Fitlm

As previously noted, function *fitlm* was used in order to balance out the weight of the manoeuvre duration. Model used is (6.10) and the results are shown in Table 6.5. To determine if covariate is significant, in statistical analysis, a term *p-value* is used. P-value tests the null hypothesis that the specified coefficient is equal to zero. This function has a 5% significance level, so coefficients for values of $p < |0.05|$ are significant, meaning that they reject the null hypothesis.
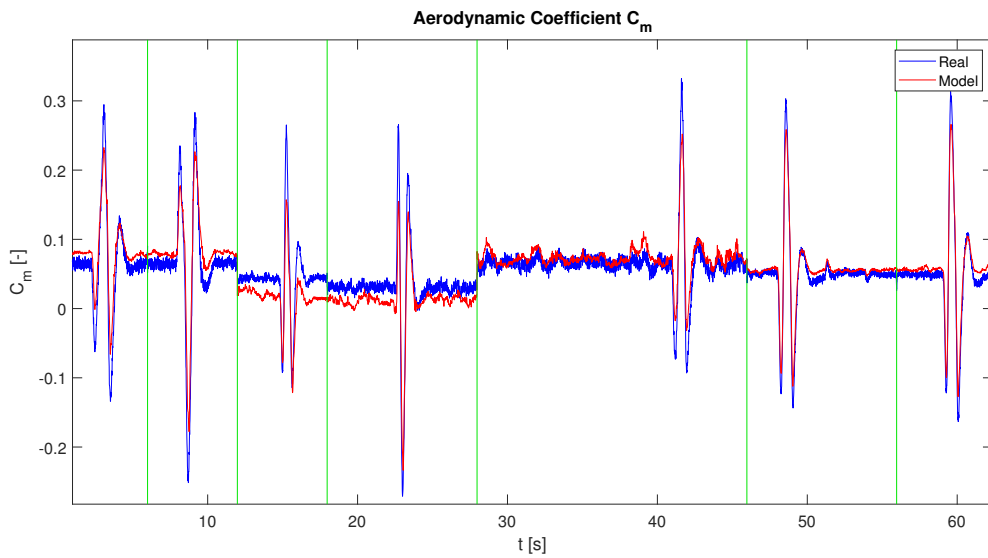

Figure 6.7: C_m model, *fitlm*, short period manoeuvres

Table 6.5: C_m estimated parameters, *fitlm*

Parameter	Value	Unit	Standard error	p-value
C_{m_0}	0.14384	–	0.00051704	0
$C_{m,\alpha}$	−0.94675	1/rad	0.0036623	0
$C_{m,q}$	−11.99	–	0.069044	0
C_{m,δ_e}	−1.8633	1/rad	0.0052068	0
C_{m,C_T}	0.33985	–	0.0021565	0

Best matching proved to be for model described by equation (6.11). This model should be used as basis for future work.

6.4.2. Lift coefficient

Besides phugoid and stall manoeuvres, model included climb manoeuvres. Model can be seen in (6.13) and the matching with real value in Figure 6.8.

$$C_L = C_{L_0} + C_{L,\alpha}\alpha + C_{L,q}q^* + C_{L,\delta_e} + C_{L,C_T}C_T \tag{6.13}$$

Model is shown on five phugoids, five stall and three climb manoeuvres, in this order. Matching of the estimated value with measurement is adequate. Again, one has to be careful when looking at the nonlinear area of stall. In fourth stall manoeuvre there is an offset at the beginning of manoeuvre which automatically brings errors in regression. Additional two plots will be shown that enhance phugoids and climbs, figures 6.9 and 6.10. Given that all manoeuvres are approximately the same duration, there is no need to develop a model using *fitlm* function.
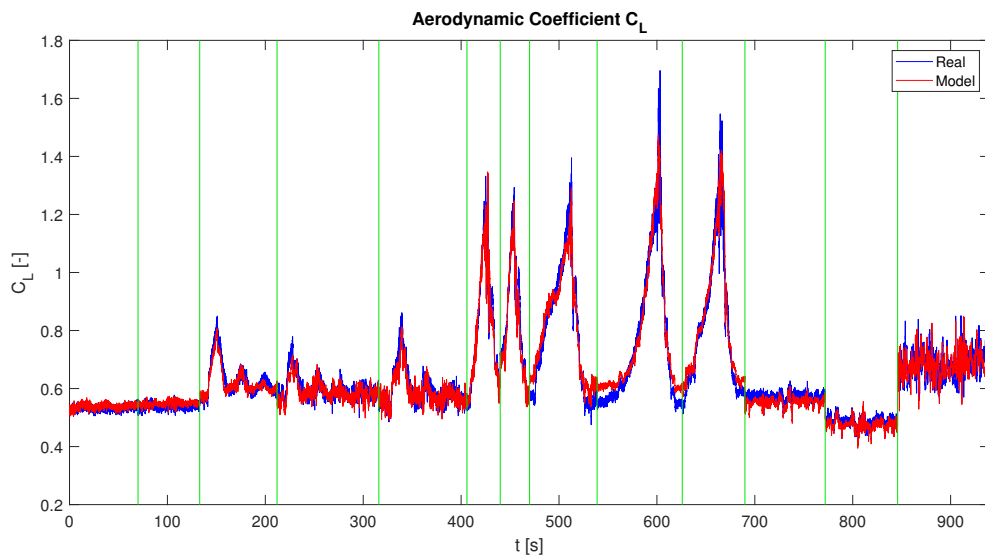

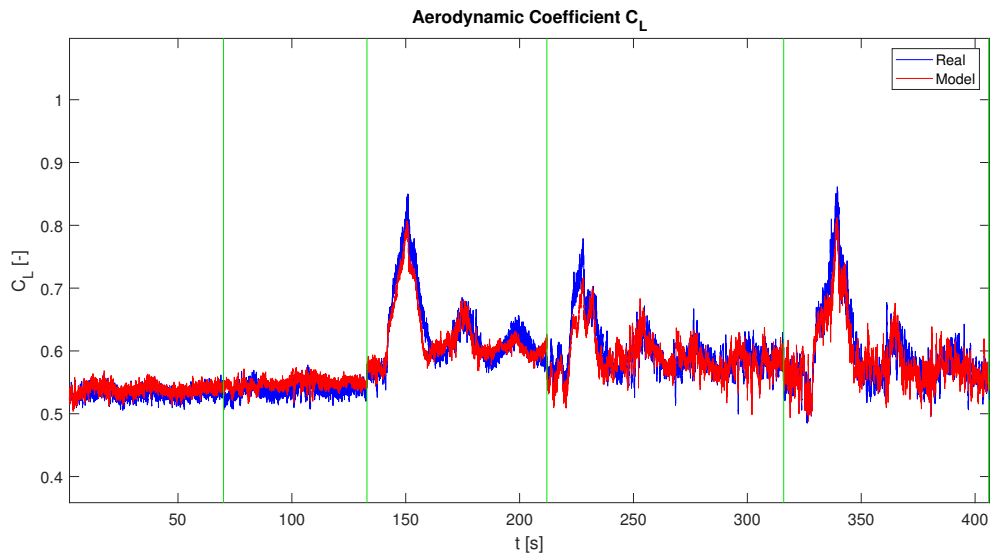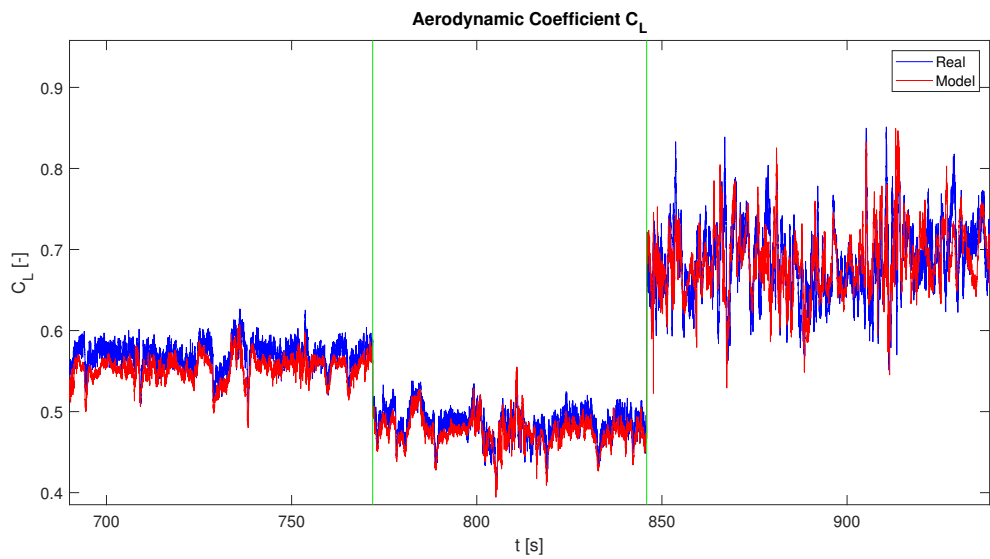Figure 6.8: C_L model for span of phugoid, stall and climb manouvres

Figure 6.9: C_L model, phugoid manoeuvres

Figure 6.10: C_L model, climb manoeuvres

Table 6.6 contains information of estimated parameters. All the derivatives are positive and of reasonable value.

Table 6.6: C_L estimated parameters

Parameter	Value	Unit	Relative error [%]
C_{L_0}	0.020742	–	3.99
$C_{L,\alpha}$	3.6903	1/rad	0.16
$C_{L,q}$	29.506	–	0.63
C_{L,δ_e}	0.52273	1/rad	1.69
C_{L,C_T}	0.0012584	–	1.70
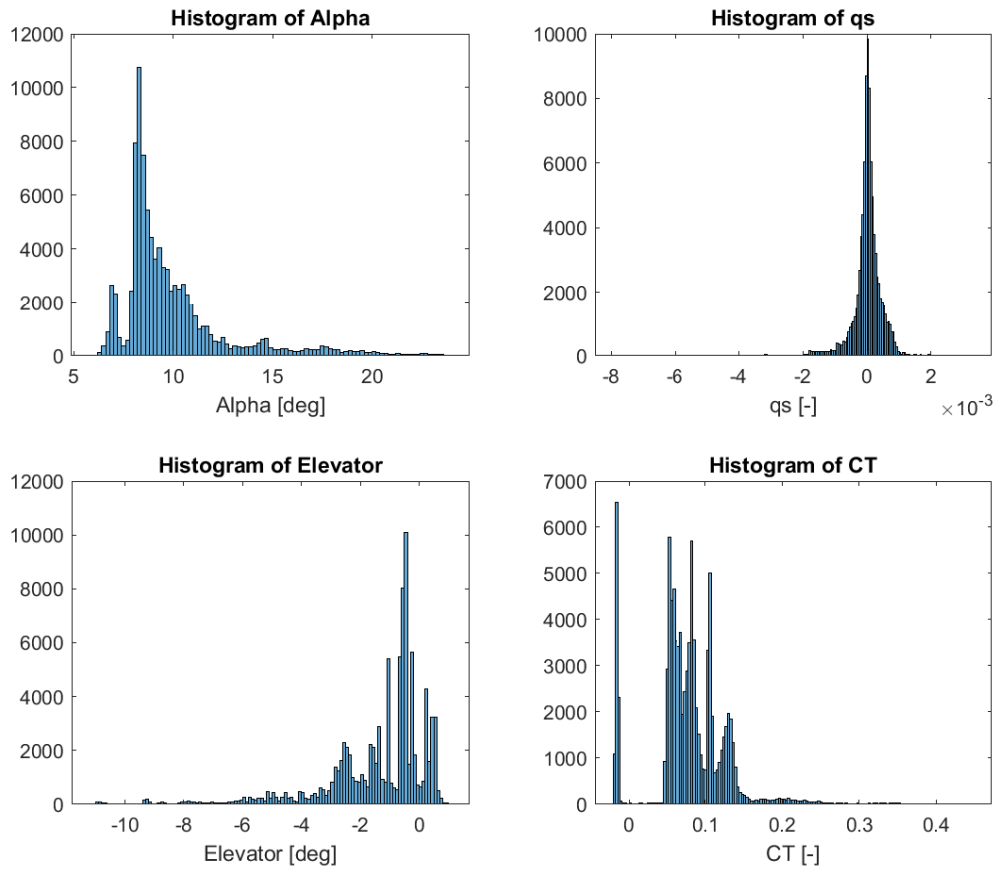
Figure 6.11: C_L predictors histogram

Predictor distributions again, like in section 6.4.1., show right skewness of α and left skewness of δ_e with high concentration of q^*, Figure 6.11. Also, residual plot did not

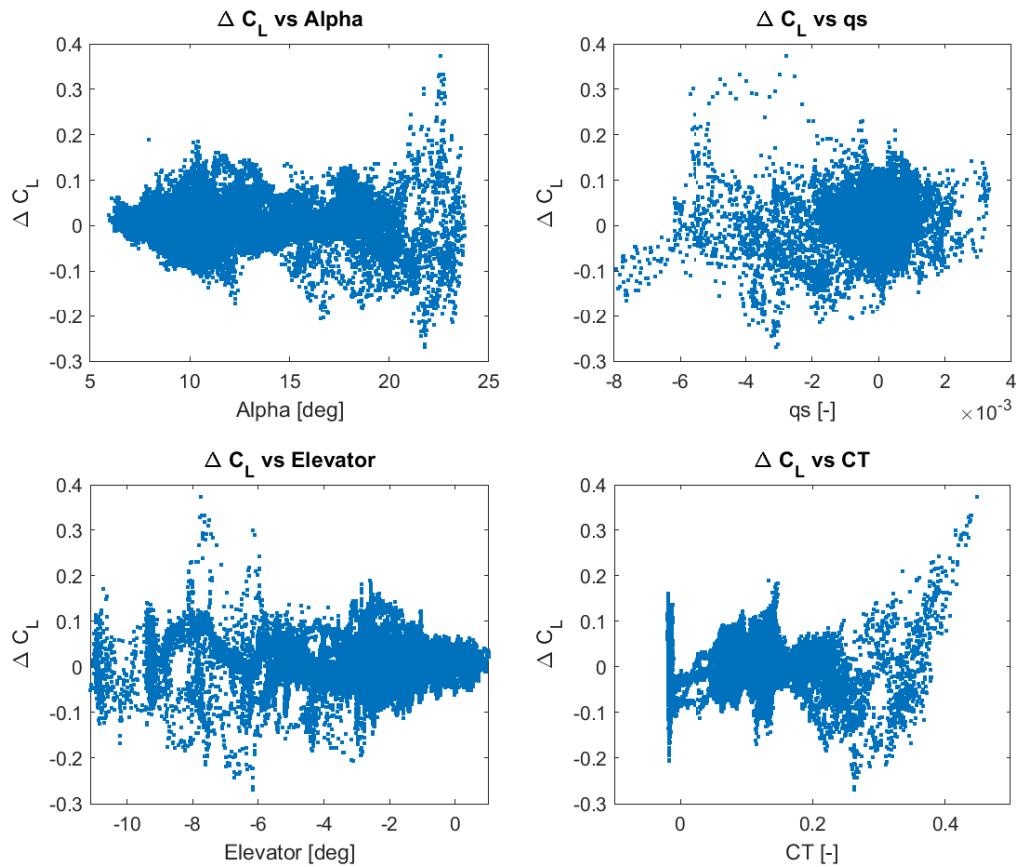show any visible pattern, so no further model expansion was done.

Figure 6.12: C_L residuals versus predictor variables

Lift coefficient functions of predictors are shown in Figure 6.13. As all terms in equation (6.13) are linear and with parameters being positive, only positive slope lines are expected. Since there are no nonlinear terms, stall curve can not show at which angle the aircraft stalls. Change of lift of the aircraft due to elevator deflection equals to change in lift force acting on tail. So for negative elevator deflection there is negative lift coefficient, which results in a force that pushes the tail down. With increasing normalized pitch rate and thrust coefficient, aerodynamic lift coefficient also increases.
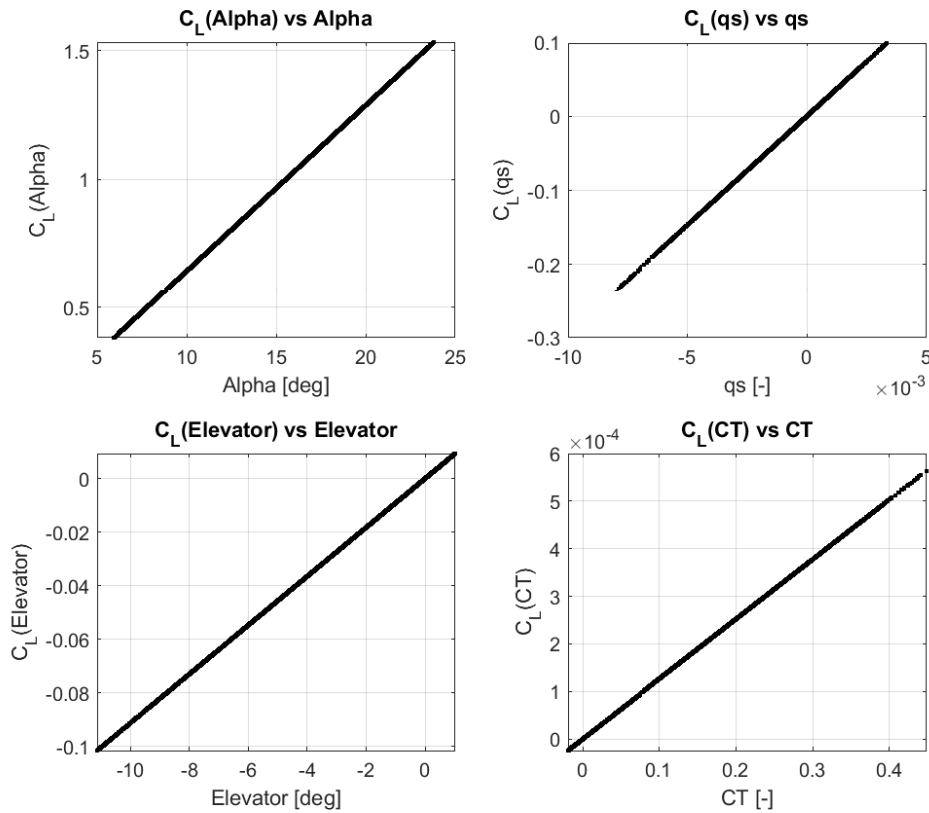
Figure 6.13: C_L predictors functions

6.5. Drag coefficient

Estimation of the parameters was done using all manoeuvres. For this case angular rates can be neglected, as well as control surfaces deflections. Derivatives of angle of attack $\dot{\alpha}$ and angle of sideslip $\dot{\beta}$ also are neglected. However, effects of AoA and AoS are highly present and both terms were introduced as quadratic. Estimation results are presented on five phugoid, four stalls and six steady heading steady sideslip manoeuvres in Figure 6.14.

$$C_D = C_{D_0} + C_{D,\alpha^2}\alpha^2 + C_{D,\beta^2}\beta^2 + C_{D,C_T}C_T \tag{6.14}$$
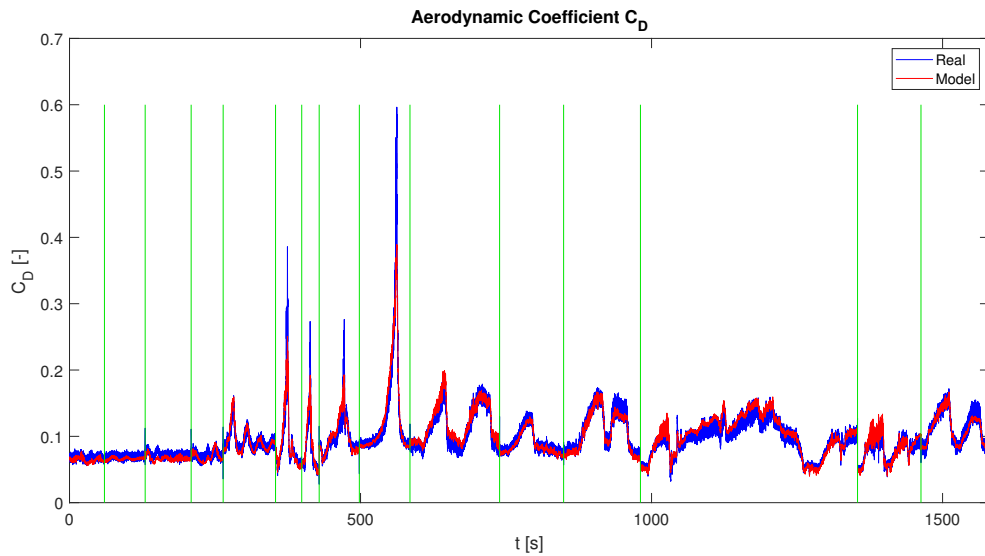
Figure 6.14: C_D model for span of phugoid, stall and shss manoeuvres

As it is expected all parameters, listed in Table 6.7, are positive.

Table 6.7: C_D estimated parameters

Parameter	Value	Unit	Relative error [%]
C_{D_0}	0.021746	–	0.17
C_{D,α^2}	1.3457	$1/\mathrm{rad}^2$	0.07
C_{D,β^2}	0.21629	$1/\mathrm{rad}^2$	0.16
C_{D,C_T}	0.33842	–	0.09

When examining residual plots, Figure 6.15, a pattern in ΔC_D vs α^2. Expanding the model, for example with $C_{D,\alpha^4}\alpha^4$ according to the residual plot, is done to improve matching of estimated value with the measurement. This model is represented with equation (6.15).
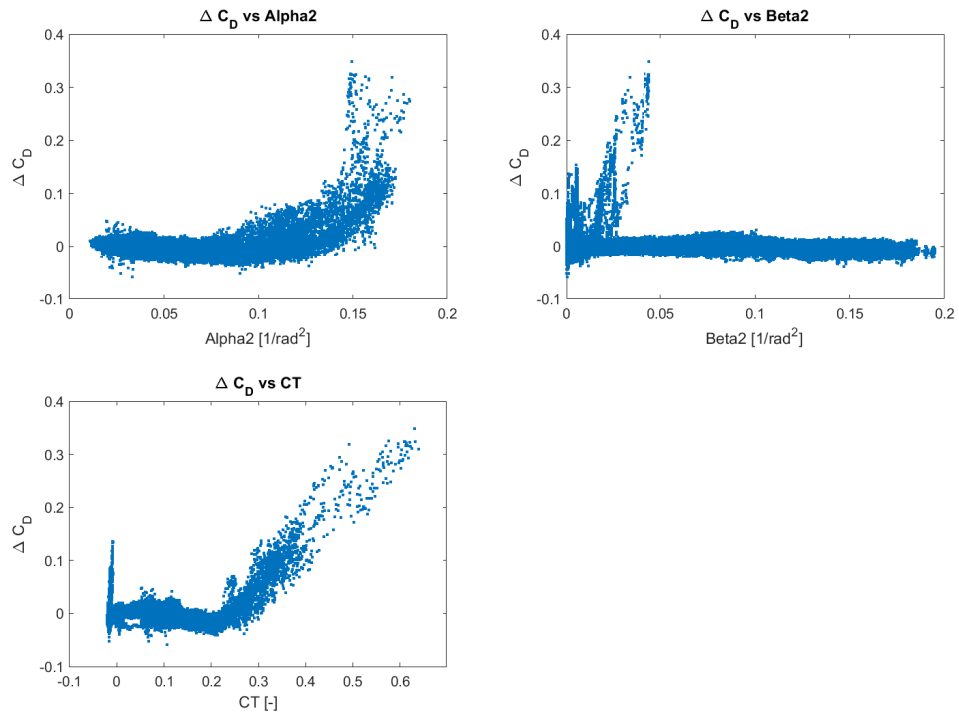
Figure 6.15: C_D residuals versus predictor variables
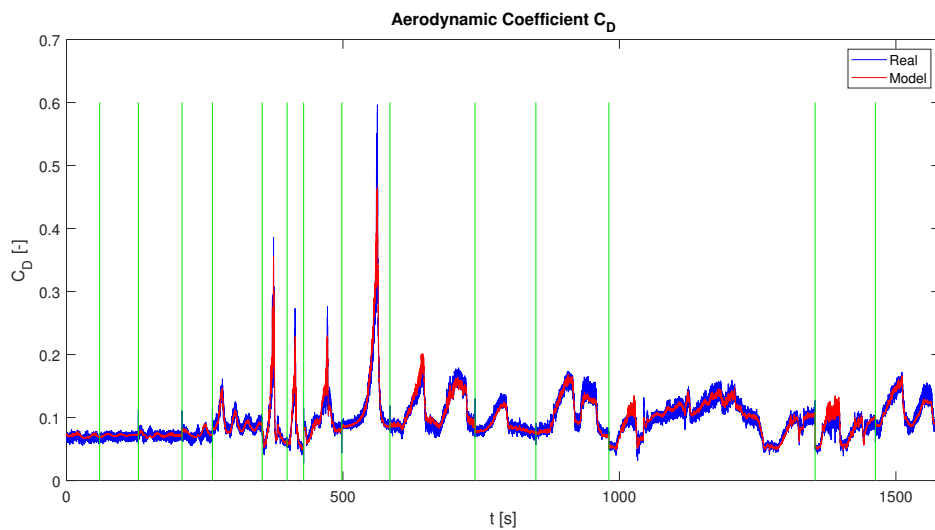
Figure 6.16: C_D expanded model for span of phugoid, stall and shss manoeu-
vres

$$C_D = C_{D_0} + C_{D,\alpha}\alpha + C_{D,\beta^2}\beta^2 + C_{D,\alpha^4}\alpha^4 + C_{D,C_T}C_T \tag{6.15}$$

Expanded model values are shown in Table 6.8 and estimation results are presented in Figure 6.16 for the same span of phugoid, stall and shss manoeuvres. All values are positive, contributing to drag when variable increases.

Table 6.8: C_D expanded model estimated parameters

Parameter	Value	Unit	Relative error [%]
C_{D_0}	0.048162	–	0.11
C_{D,α^2}	0.15122	$1/\text{rad}^2$	1.52
C_{D,β^2}	0.28059	$1/\text{rad}^2$	0.11
C_{D,C_T}	0.32272	–	0.08
C_{D,α^4}	9.7931	$1/\text{rad}^4$	0.18

With the expanded model, the matching did not improve. Being in low values of C_D, estimated value follows real value better, however on high peaks it tends to overshoot as it can be seen for span of phugoid, stall and shss manoeuvres, visible in Figure 6.17. For this reason this model, (6.15), should not be taken into account for further analysis.
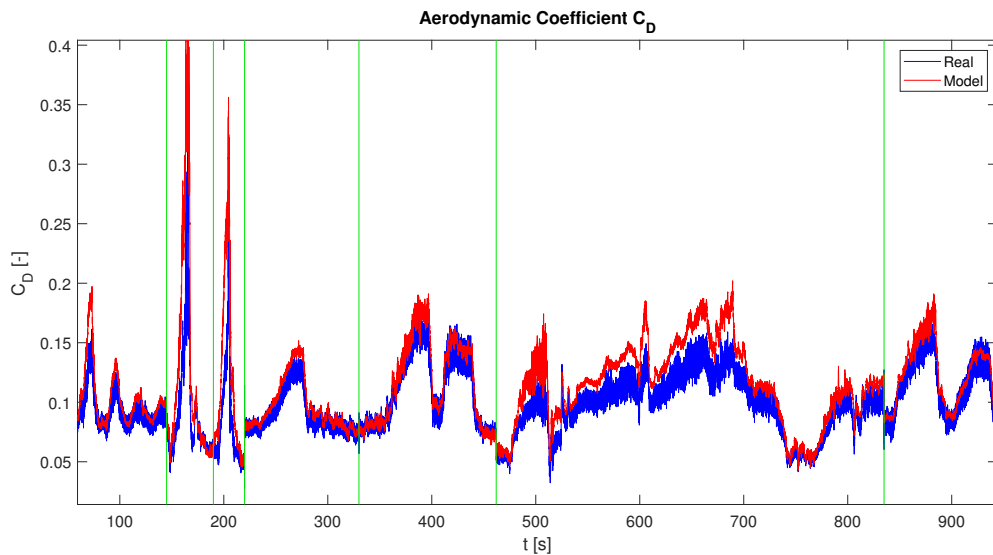
Figure 6.17: C_D model overshooting

In the end drag coefficient functions of predictors for model (6.14) are shown in Figure 6.18. With increasing angle of attack aerodynamic drag coefficient increases quadratically and for thrust coefficient linearly. Airplane is symmetric, that is why aerodynamic drag coefficient is the same for either positive or negative angle of sideslip. Obviously minimum drag is when the AoS is zero.

Figure 6.18: C_D predictors functions

7 | Conclusion

Purpose of this thesis was to improve the existing basic aerodynamic coefficient models. As the work done in this thesis is a con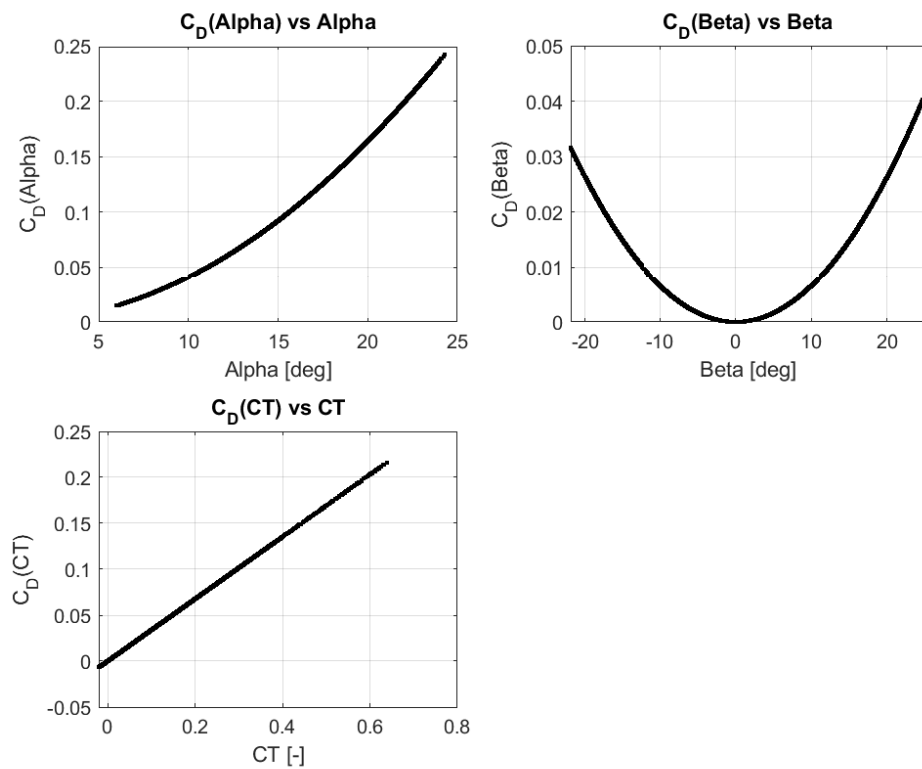tinuation of work on a project, besides of verifying all the data and scripts being used, additional steps had to be made before aerodynamic modelling. All work was done in a way that successors working on this project can easily pick up from this point.

Firstly, all the data and scripts were examined and verified, along with that raw data was reprocessed. After that, error of measuring unit due to misalignment was corrected making sure that the data is accurate for further work.

Reconstructing the airplane trajectory as accurately as possible validates measured data for aerodynamic modelling, eliminating corruptions (errors). It is a time exhausting iterative process based on Output-Error Method. Three sensor error models are developed and the results proved that the trajectory was reconstructed with sufficient accuracy. In this project reconstructed data was corrected to match the measured one, so in the end an inversion of the developed models was required. The adopted models are:

- Angle of sideslip error model (equation (5.18), Table 5.3)

- Dynamic pressure error model (equation (5.19), Table 5.1)

- Angle of attack error model (equation (5.20), Table 5.2)

At-last existing aerodynamic models of longitudinal stability were improved. The models are now more detailed and of higher accuracy. Effect of each predictor in the models was examined and stated. Modelling is based on linear regression and the most commonly

used algorithm Ordinary-Least Squares. Based on presented longitudinal aerodynamic coefficients analysis following models are developed:

- Pitching moment coefficient C_m (equation (6.11), Table 6.4)

- Lift coefficient C_L (equation (6.13), Table 6.6)

- Drag coefficient C_D (equation (6.14), Table 6.7)

For the continuation of work on this project, lateral stability coefficient models need to be developed in the same workflow. In addition to that, developed model can be further expanded. For example, in pitching moment coefficient model, angle of attack derivative term addition could estimation value to reach the peaks in short period manoeuvres. Also, the whole model could possibly be upgraded by developing nonlinear models. Completion of the aerodynamic model allows the project to proceed to it's final stages, which would be implementation of the model in ReDSim simulator.

A | Appendix

A.1. Flight Test Data

- Folder: *Data*

  ○ Folder: *Flights*

  ○ Folder: *Manoeuvres*

A.1.1. Data check

- Folder: *Data_Check*

  – *data_check.m*

A.2. Data Correction

- Folder: *Utilities*

  – *getCorrEulAng.m*

  – *getCorrSens.m*

A.3. Flight Path Reconstruction

- Folder: *FPR*

- ○ Folder: *fitlab*

    – *fitlab.m*

- Folder: *Utilities*

    – *compileCorrADB.m*

    – *getADBCorr.m*

    – *plotADBCorr.m*

A.4. Parameter Estimation

- Folder: *Utilities*

    – *AeroCoeff_fitlm.m*

    – *CD_estimation.m*

    – *CL_estimation.m*

    – *Cm_estimation.m*

    – *ols_fit.m*

    – *plot_AeroCoeff_functions.m*

    – *plot_AeroCoeff_model.m*

    – *plot_AeroCoeff_param_histogram.m*

    – *plot_AeroCoeff_residuals.m*

Bibliography

[1] Kevin Spillman. Flight Testing of a General Aviation Aircraft and Simulation Model Development. Master's thesis, Zurich University of Applied Sciences, 2019.

[2] Flavio Ferrari. Flight Testing of a General Aviation Aircraft and Aerodynamic Model Estimation. Master's thesis, Zurich University of Applied Sciences, 2019.

[3] David Haber-Zelanto. Aerodynamic Coefficients Estimation of a General Aviation Airplane from Flight Test Data. Master's thesis, Faculty of Mechanical Engineering and Naval Architecture, University of Zagreb, 2021.

[4] Warrior III PA-28-161 Pilot's Operating Handbook and FAA Approved Airplane Flight Manual. 2015.

[5] Ravindra V. Jategaonkar. *Flight Vehicle System Identification - A Time Domain Methodology.* Progress in Astronautics and Aeronautics, Volume 245. American Institute of Aeronautics and Astronautics, second edition, 2015.

[6] Vladislav Klein and Eugene A. Morelli. *Aircraft System Identification: Theory And Practice.* AIAA (American Institute of Aeronautics and Astronautics), 1st edition, 2006.

[7] S. Janković. *Mehanika leta zrakoplova.* Sveučilište u Zagrebu, Fakultet Strojarstva i Brodogradnje, 2002.

[8] Milan Vrdoljak S. Janković, Todor Kostić. *Stabilnost i upravljivost zrakoplova.* Sveučilište u Zagrebu, Fakultet Strojarstva i Brodogradnje, 2011.

[9] Susanne Seher-Weiss. *User's Guide FITLAB - Parameter Estimation Using MAT-LAB - Version 2.3.* Deutsches Zentrum für Luft- und Raumfahrt (DLR), Institut für Flugsystemtechnik, 2014-02-14.

[10] Marcel Dettling. *Applied Statistical Regression.* Zurich University of Applied Sciences, Institute for Data Analysis and Process Design, 2021.

[11] Eugene A. Morelli Jared A. Grauer and Daniel G. Murri. Flight-test techniques for quantifying pitch rate and angle-of-attack rate dependencies. *JOURNAL OF AIRCRAFT*, 54(6), November 2017.